
Goal-Oriented Lower-Tail Calibration of Gaussian Processes for Bayesian Optimization

Aurélien Pion^{1,2} Emmanuel Vazquez²

Abstract

Bayesian optimization (BO) selects evaluation points for expensive black-box objectives using Gaussian process (GP) predictive distributions. Kernel choice and hyperparameter selection can lead to miscalibrated predictive distributions and an inappropriate exploration–exploitation trade-off. For minimization, sampling criteria such as expected improvement (EI) depend on the predictive distribution below the current best value, so lower-tail miscalibration directly affects the sampling decision. This article studies goal-oriented calibration of GP predictive distributions below a low threshold t in the noiseless setting, for standard GP models with hyperparameters selected by maximum likelihood. A framework for predictive reliability below t is introduced, based on two notions of spatial calibration: occurrence calibration over the design space and thresholded μ -calibration on sublevel sets of the form $\{x \in \mathbb{X}, f(x) \leq t\}$. Building on this framework, we propose tcGP, a post-hoc method that calibrates GP predictive distributions below t , and we show that the resulting EI-based global optimization algorithm remains dense in the design space. Experiments on standard benchmarks show improved lower-tail calibration and BO performance relative to standard GP models and globally calibrated GP models.

1. Introduction

This article considers the minimization of an *expensive-to-evaluate* function f defined over a design space $\mathbb{X} \subset \mathbb{R}^d$, with noiseless evaluations (a query at x returns $f(x)$ exactly). A widely used approach for this setting is Bayesian

optimization (BO) (see, e.g., Mockus et al., 1978; Jones et al., 1998; Villemonteix et al., 2009; Srinivas et al., 2010). In the single-objective setting, BO aims at identifying a global minimizer $x^* \in \arg \min_{x \in \mathbb{X}} f(x)$ using a limited evaluation budget, modeling f a priori as a Gaussian process (GP), denoted by $\xi \sim \text{GP}(m, k)$, with mean function m and covariance kernel k . Given an initial set of evaluations, the GP posterior yields predictive distributions for f : for each $x \in \mathbb{X}$, it provides a predictive cumulative distribution function (CDF) $\hat{F}_n(\cdot | x)$ for the unknown value $f(x)$ at iteration n . At each iteration, the next evaluation point is selected by maximizing a *sampling criterion*, also referred to as an *acquisition function*, that depends on this predictive distribution, such as expected improvement (EI) (Mockus et al., 1978; Schonlau & Welch, 1996).

To avoid unnecessary evaluations of f , the predictive distributions should reflect uncertainty at each iteration n in order to guide the selection of new evaluation points toward the minimum. In practice, GP predictive distributions are sensitive to kernel choice and hyperparameter misspecification, which can lead to over- or under-estimated uncertainty (Pion & Vazquez, 2025). Such misspecification can mislead the sampling criterion and substantially degrade the performance of BO (Bogunovic & Krause, 2021).

While improving GP predictive performance over the whole domain is desirable (Bogunovic & Krause, 2021; Guo et al., 2021; Tuo & Wang, 2022; Deshpande et al., 2024; Tom et al., 2025), BO can benefit from *goal-oriented* prediction, in particular from accurate predictions below a low threshold $t \in \mathbb{R}$. Here, t is a data-driven threshold chosen in the lower tail of the observations, e.g., as an empirical δ -quantile of the observed responses for some $\delta \in (0, 1]$. Along these lines, Petit et al. (2025) propose the *relaxed Gaussian process* (REGP), a GP-based model designed to improve predictive accuracy below t . REGP builds on GP interpolation and relaxes the interpolation constraints above t to improve predictions below this level. They report improved BO performance compared with standard GP-based methods.

Following the idea of goal-oriented prediction below a threshold t , this work investigates whether BO can benefit from probabilistic models that are *calibrated below a low*

¹Transvalor S.A., Biot, France ²Univ. Paris-Saclay, CNRS, CentraleSupélec, L2S, Gif-sur-Yvette, France. Correspondence to: Emmanuel Vazquez <emmanuel.vazquez@centralesupelec.fr>.

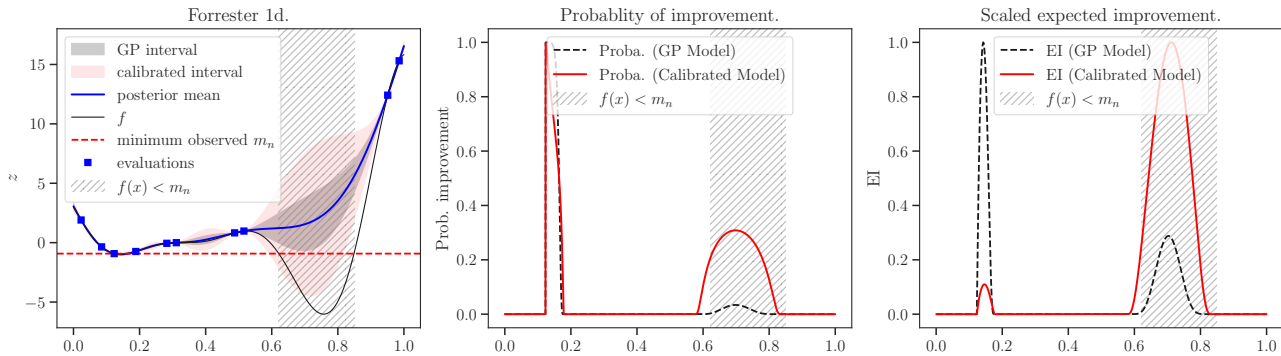


Figure 1. Comparison between a standard GP and a model calibrated below $q_{\delta,n}$ (TCGP), with $\delta = 0.3$, on a standard one-dimensional test function and with $n = 10$ evaluations. Left: observations with GP predictions; the current design does not include a point near the global minimizer. Middle: probabilities of improvement $\hat{F}_n^{(0)}(m_n | x)$ (GP, black) and $\hat{F}_n^{(1)}(m_n | x)$ (TCGP, red), where $m_n = \min_{i \leq n} f(X_i)$. Right: EI for the GP and TCGP, each rescaled by its maximum over \mathbb{X} . Here, calibration raises the predicted probability of improvement in the sparsely sampled region near the global minimizer, where the current design has no evaluation, and EI increases there accordingly. This exploration behavior seems appropriate in this example.

threshold t , and compares them with standard GP models and with post-hoc globally calibrated GP predictive distributions over \mathbb{X} . By calibration below t , we mean that the lower tail of the predictive CDFs $\hat{F}_n(\cdot | x)$ is reliable for inputs drawn from μ . The average probability assigned to the event $f(X) \leq t$, with $X \sim \mu$, matches its frequency, and, on the sublevel set $\{f(X) \leq t\}$, the transformed lower-tail values have the correct distribution.

Consider Figure 1, which compares a GP model with hyperparameters selected by maximum likelihood and a model calibrated below the empirical δ -quantile $q_{\delta,n}$ ($\delta = 0.3$), on a standard one-dimensional test function (from Forrester et al., 2008). The middle panel displays the predicted probabilities of improvement

$$\hat{F}_n^{(j)}(m_n | x), \quad j \in \{0, 1\}, \quad (1)$$

where $\hat{F}_n^{(j)}(\cdot | x)$ is the predictive CDF at x , with $j = 0$ for the GP and $j = 1$ for the calibrated predictive distribution, and $m_n = \min_{i \leq n} f(X_i)$. In the shaded region, the GP assigns low lower-tail probabilities despite sparse sampling, while the calibrated model assigns larger values, which raises EI in that region. This example is constructed to illustrate the issue in a minimal setting. In higher dimensions, similar behavior can arise when the selected hyperparameters lead to local overconfidence in sparsely sampled regions, with underestimated lower-tail probabilities and reduced exploration. This motivates lower-tail calibration of predictive distributions, since improvement-based sampling criteria are sensitive to tail miscalibration.

This work makes two contributions. Inspired by the notion of *probabilistic tail calibration* introduced by Allen et al. (2025), we define two notions of *spatial calibration below t* : *occurrence calibration* over \mathbb{X} and *thresholded μ -calibration* on the sublevel set $\{x \in \mathbb{X}, f(x) \leq t\}$.

A *post-hoc* calibration method for GP predictive distributions is also introduced, inspired by Pion & Vazquez (2025), termed *calibrated prediction below t for GPs* (TCGP). Standardized residuals are modeled with a parametric generalized normal family, with parameters selected by optimizing a criterion targeting spatial calibration below t . The resulting predictive distributions are used in BO with the EI criterion. Analytical expressions for EI with TCGP are derived, together with a convergence result. We also report additional experiments using the UCB sampling criterion in the appendix.

We evaluate TCGP and REGP empirically and find improved lower-tail calibration and BO performance relative to standard GP models, globally calibrated GP models (Pion & Vazquez, 2025), sequential calibration (Deshpande et al., 2024), and variants that target only one of the two calibration notions.

Section 2 reviews related work. Sections 3–5 introduce the setting, TCGP, and the TCGP-based EI algorithm. Section 6 reports experiments.

2. Related Work

Calibration and goal-oriented prediction Classical notions of calibration, such as probabilistic calibration and proper scoring rules, typically address *global* calibration of predictive distributions over the domain \mathbb{X} (Gneiting et al., 2007; Gneiting & Resin, 2023; Pion & Vazquez, 2025). Calibration in BO with non-i.i.d. data is studied by Deshpande et al. (2024), who propose online recalibration and conformal procedures to maintain quantile calibration within the BO loop. Sahoo et al. (2021) introduced *threshold calibration* for decision-making applications and proposed a method for obtaining reliable estimates of threshold-based

losses. Their notion is closely related to thresholded μ -calibration considered here. This article is formulated in a spatial setting over \mathbb{X} and considers two notions of calibration below t : occurrence calibration over \mathbb{X} and thresholded μ -calibration on the sublevel set $\{x \in \mathbb{X}, f(x) \leq t\}$. Friedli et al. (2025) introduced a GP-based sequential design method built from the threshold-weighted continuous ranked probability score (twCRPS), and applied it to excursion set estimation.

Conformal prediction. Conformal prediction (CP) provides finite-sample coverage guarantees for a new response when the data are exchangeable (Vovk et al., 2005). Conformal predictive systems (CPS) extend CP to full predictive distributions (Vovk et al., 2019). CPS have been applied to GP interpolation by Pion & Vazquez (2025). Goal-oriented CP methods target coverage on selected subsets of inputs (Zhang & Candès, 2024; Jin & Ren, 2025), but typically yield piecewise-constant predictive distributions and still rely on exchangeability. CP has also been used for sequential optimization with noisy evaluations (Stanton et al., 2023; Kim et al., 2025). These approaches are not tailored to lower-tail BO criteria and can be computationally demanding. In this work, we adopt a GP-specific post-hoc calibration approach inspired by Pion & Vazquez (2025) and adapt it to prediction below a threshold.

Alternative BO formulations. Misspecification in BO and sequential decision-making has been studied by Neiswanger & Ramdas (2021), who analyzed the impact of global variance misspecification. Several works also modify the probabilistic model or the sampling criterion to improve BO, without targeting calibration of predictive lower-tail probabilities. Picheny et al. (2019) considers BO with *ordinal observations* (e.g., pairwise preferences or rank information) and builds on variational ordinal GP regression (Chu & Ghahramani, 2005). Picheny et al. (2022) focuses on quantiles and expectiles of the predictive distribution.

3. Background and Problem Setup

3.1. Problem Setting and Notation

Bayesian optimization proceeds sequentially. We start from an initial dataset $\mathcal{D}_{n_0} = \{(X_i, Z_i)\}_{i=1}^{n_0}$, where $Z_i = f(X_i)$ and the inputs X_i are drawn according to an initial design measure μ_0 on \mathbb{X} . We then run $n - n_0$ additional BO iterations, $n > n_0$. For $i > n_0$, the design points X_i are selected by maximizing a sampling criterion, so their distribution is determined by the BO strategy. Using the dataset \mathcal{D}_n we construct a family of predictive CDFs $\hat{F}_n(\cdot | x)$ for $x \in \mathbb{X}$. This family is used to define the sampling criterion and thereby governs the choice of the next point X_{n+1} to evaluate f .

We focus on the EI sampling criterion in this work. (We also consider the UCB policy and report complementary results in Appendix F.6.2.) For the family of predictive densities $\hat{p}_n(\cdot | x)$, with $x \in \mathbb{X}$, the EI is defined as

$$\rho_n(x) = \int_{\mathbb{R}} (m_n - z)_+ \hat{p}_n(z | x) dz,$$

where $m_n = \min(f(X_1), \dots, f(X_n))$. EI is primarily controlled by the predicted probability mass below m_n and the shape of the predictive CDF on $(-\infty, m_n]$, motivating calibration specifically in the lower tail rather than globally.

Consider a fixed reference measure μ on \mathbb{X} used to define and assess spatial calibration (e.g., uniform on \mathbb{X}). The measure μ may coincide with μ_0 , but it is fixed independently of the BO policy. For fixed n and \mathcal{D}_n , let $X \sim \mu$ be an auxiliary draw, independent of \mathcal{D}_n . We write $P_n(\cdot) := P_X(\cdot)$ and $E_n(\cdot) := E_X(\cdot)$ for probability and expectation with respect to this auxiliary draw $X \sim \mu$, with \mathcal{D}_n fixed. The subscript indicates that the integrands depend on \mathcal{D}_n through $\hat{F}_n(\cdot | X)$.

3.2. A Generalized Normal Distribution Model for Prediction Errors

In this section, we depart from the Bayesian interpretation of the GP model. The function f is treated as fixed and deterministic, and the GP formalism is used only as a device to construct, from \mathcal{D}_n , a predictive mean $f_n(\cdot)$ and a predictive variance $\sigma_n^2(\cdot)$. We retain from this construction the associated Gaussian predictive distributions $\hat{F}_n^{\text{GP}}(z | x) = \Phi((z - f_n(x))/\sigma_n(x))$, $x \in \mathbb{X}$, $z \in \mathbb{R}$, where Φ is the standard normal CDF, with the convention $\hat{F}_n^{\text{GP}}(z | x) = \mathbf{1}\{z \geq f_n(x)\}$ when $\sigma_n(x) = 0$.

To assess deviations from this Gaussian predictive distribution for $X \sim \mu$, define the standardized prediction error

$$R_n(x, f(x)) = \frac{f(x) - f_n(x)}{\sigma_n(x)}, \quad (2)$$

with $R_n(x, f(x)) = 0$ if $\sigma_n(x) = 0$. Under the GP model, for any fixed x with $\sigma_n(x) > 0$, the conditional distribution of $(\xi(x) - f_n(x))/\sigma_n(x)$ given \mathcal{D}_n is standard normal. In contrast, since f is deterministic, $R_n(X, f(X))$ is random only through $X \sim \mu$ and its distribution need not be Gaussian.

Following Pion & Vazquez (2025), we model $R_n(X, f(X))$ with a generalized normal (GN) family, denoted by $\mathcal{GN}(\beta, l, \lambda)$ with $\beta > 0$, $\lambda > 0$, and $l \in \mathbb{R}$ (density recalled in Appendix A). The parameter l is a location parameter, λ controls dispersion, and β controls tail decay; $\beta = 2$ corresponds to the Gaussian case and $\beta = 1$ to the Laplace case.

For any $x \in \mathbb{X}$ and parameters β, l, λ , we define the predic-

tive CDF

$$\hat{F}_n^{\beta,l,\lambda}(z | x) = \Theta_{\beta,l,\lambda}\left(\frac{z - f_n(x)}{\sigma_n(x)}\right), \quad z \in \mathbb{R}, \quad (3)$$

with the convention $\hat{F}_n^{\beta,l,\lambda}(z | x) = \mathbf{1}\{z \geq f_n(x)\}$ when $\sigma_n(x) = 0$, where $\Theta_{\beta,l,\lambda}$ is the CDF of $\mathcal{GN}(\beta, l, \lambda)$.

Pion & Vazquez (2025) fix $l = 0$ and select (β, λ) via a Bayesian procedure inspired by tolerance-interval constructions (Meeker et al., 2017), targeting μ -probabilistic calibration of the predictive distribution over \mathbb{X} . The resulting method is the *Bayesian calibration of residuals for GPs* (BCRGP).

4. Spatial Calibration below a Threshold

4.1. Statistical Formulation

In this section, we introduce notions of calibration below a threshold $t \in \mathbb{R}$ with respect to a fixed measure μ on \mathbb{X} . For a given n , consider predictive CDFs $\hat{F}_n(\cdot | x)$, $x \in \mathbb{X}$, such that for μ -almost all x the map $z \mapsto \hat{F}_n(z | x)$ is continuous and strictly increasing on \mathbb{R} . We assess calibration of the predictive distributions in the lower tail up to t .

For $z \leq t$, the predictive CDF can be decomposed as

$$\hat{F}_n(z | x) = \hat{F}_n(t | x) \hat{F}_{n,t}(z | x), \quad (4)$$

where $\hat{F}_n(t | x)$ is the predicted probability mass below t , and $\hat{F}_{n,t}(\cdot | x)$ is the predictive CDF truncated below t , such that, for all $z \leq t$,

$$\hat{F}_{n,t}(z | x) = \mathbb{P}_{\hat{F}_n(\cdot | x)}(Z \leq z | Z \leq t) = \frac{\hat{F}_n(z | x)}{\hat{F}_n(t | x)}, \quad (5)$$

with $Z \sim \hat{F}_n(\cdot | x)$. We therefore introduce two complementary notions: *thresholded μ -calibration*, targeting the shape of the predictive distribution within the thresholded region through $\hat{F}_{n,t}$, and *occurrence calibration*, targeting the probability mass assigned to the region through $\hat{F}_n(t | x)$ averaged over \mathbb{X} .

This decomposition parallels the severity–occurrence split in probabilistic tail calibration (Allen et al., 2025). In that setting, *severity* refers to calibration of the conditional distribution given $Z \leq t$, and *occurrence* refers to calibration of the predictive probability of the event $\{Z \leq t\}$. The definitions introduced here adapt this split to a spatial setting over \mathbb{X} with a fixed threshold t .

Thresholded μ -calibration. Thresholded μ -calibration is a tail version of μ -probabilistic calibration (Pion & Vazquez, 2025), obtained by restricting attention to the thresholded region $\{f(X) \leq t\}$ for an auxiliary draw $X \sim \mu$.

Recall the probability integral transform (PIT), which motivates the definition below: if a random variable Z has a continuous and strictly increasing CDF F , then the PIT $F(Z)$ is uniformly distributed on $[0, 1]$. Hence, if a predictive CDF \hat{F} matches the distribution of Z , then the PIT $\hat{F}(Z)$ is uniform: departures from uniformity indicate miscalibration. Pion & Vazquez (2025) extend this idea to a spatial (design-marginal) setting by introducing the μ -PIT, based on an auxiliary draw $X \sim \mu$. Here we apply the same idea conditionally on $\{f(X) \leq t\}$ through the truncated CDF $\hat{F}_{n,t}(\cdot | X)$.

Assume that $\mu(\{x \in \mathbb{X} : f(x) \leq t\}) > 0$ and $\mu(\{x \in \mathbb{X} : f(x) = t\}) = 0$. The second condition avoids an atom at one in the thresholded PIT. The μ -probability integral transform restricted to the thresholded region (μ -tPIT) is defined by

$$U_t := \begin{cases} \hat{F}_{n,t}(f(X) | X), & f(X) \leq t, \\ 1, & f(X) > t. \end{cases} \quad (6)$$

We say that \hat{F}_n is *μ -probabilistically calibrated below t* if $U_t | \{f(X) \leq t\}$ is uniform on $[0, 1]$. This is the thresholded analogue of μ -probabilistic calibration (Pion & Vazquez, 2025): among points such that $f(X) \leq t$, the values $\hat{F}_{n,t}(f(X) | X)$ should be uniformly distributed on $[0, 1]$.

For $u \in [0, 1]$, define

$$G_{\mu,t}(u) := \mathbb{P}_n(U_t \leq u | f(X) \leq t). \quad (7)$$

Then μ -probabilistic calibration below t is equivalent to $G_{\mu,t}(u) = u$ for all $u \in [0, 1]$.

Occurrence calibration. Thresholded μ -calibration constrains the distribution of $\hat{F}_{n,t}(f(X) | X)$ conditional on $\{f(X) \leq t\}$. It does not constrain the total probability mass assigned to $\{f(X) \leq t\}$, which is governed by $\hat{F}_n(t | x)$.

Let p_t denote the excursion probability for $X \sim \mu$,

$$p_t = \mathbb{P}(f(X) \leq t). \quad (8)$$

The *occurrence discrepancy* is

$$r_{t,n} = \left| p_t - \mathbb{E}_n[\hat{F}_n(t | X)] \right|, \quad X \sim \mu. \quad (9)$$

Equivalently, $p_t = \mu(\{x \in \mathbb{X} : f(x) \leq t\})$ and $\mathbb{E}_n[\hat{F}_n(t | X)] = \int_{\mathbb{X}} \hat{F}_n(t | x) \mu(dx)$. We say that \hat{F}_n is *occurrence-calibrated at threshold t* if $r_{t,n} = 0$.

4.2. Metrics for Prediction below a Threshold

We assess thresholded μ -probabilistic calibration by comparing the distribution of the μ -tPIT to the uniform distribution using the Kolmogorov–Smirnov distance. This yields

the *tKS-PIT* metric:

$$J_{\text{tKS-PIT}}(\hat{F}_n | t) := \sup_{u \in [0,1]} |G_{\mu,t}(u) - u|. \quad (10)$$

Weighted LOO μ -tPIT and tKS-PIT. The tKS-PIT and occurrence discrepancy r_t are defined with respect to the reference measure μ on \mathbb{X} . In principle, they should be evaluated on an independent dataset $(X'_j, f(X'_j))_{j=1}^L$ with $X'_j \sim \mu$. In BO, such an evaluation set is typically unavailable. We therefore rely on the observed BO data \mathcal{D}_n and use leave-one-out (LOO) predictive CDFs. Since the BO design points are not distributed according to μ in general, we also allow for reweighting to approximate μ -averages.

Let $\mathcal{D}_n = \{(X_i, Z_i)\}_{i=1}^n$ with $Z_i = f(X_i)$. For each $i \in \{1, \dots, n\}$, let $\hat{F}_{n,-i}(\cdot | x)$ denote the predictive CDF constructed from $\mathcal{D}_n \setminus \{(X_i, Z_i)\}$. Fix $t \in \mathbb{R}$.

Let $(w_i)_{i=1}^n$ be nonnegative weights and set $\tilde{w}_i = w_i / \sum_{j=1}^n w_j$. The weights are chosen so that weighted averages over (X_i) approximate μ -averages. The unweighted case corresponds to $w_i = 1$. In this work, (w_i) is obtained by density-ratio estimation based on a density estimate of the BO design distribution; details are given in Appendix E.3 (paragraph *Density-ratio estimation and weights*).

Assume that $\hat{F}_{n,-i}(t | X_i) > 0$ whenever $Z_i \leq t$. Define the LOO empirical μ -tPIT by

$$U_{t,i}^{\text{LOO}} = \begin{cases} \hat{F}_{n,-i}(Z_i | X_i) / \hat{F}_{n,-i}(t | X_i), & Z_i \leq t, \\ 1, & Z_i > t. \end{cases} \quad (11)$$

We estimate p_t using the weighted empirical frequency

$$\hat{p}_{t,n}^w = \sum_{i=1}^n \tilde{w}_i \mathbf{1}\{Z_i \leq t\}. \quad (12)$$

Assume that $\hat{p}_{t,n}^w > 0$ and define

$$G_{t,n}^{\text{LOO},w}(u) = \frac{\sum_{i=1}^n \tilde{w}_i \mathbf{1}\{Z_i \leq t\} \mathbf{1}\{U_{t,i}^{\text{LOO}} \leq u\}}{\hat{p}_{t,n}^w}. \quad (13)$$

The weighted empirical tKS-PIT metric is

$$J_{\text{tKS-PIT},n}^{\text{LOO},w}(\hat{F}_n | t) = \sup_{u \in [0,1]} \left| G_{t,n}^{\text{LOO},w}(u) - u \right|. \quad (14)$$

Weighted estimation of p_t and occurrence discrepancy.

The corresponding weighted LOO occurrence discrepancy estimator is

$$r_{t,n}^{\text{LOO},w} = \left| \hat{p}_{t,n}^w - \sum_{i=1}^n \tilde{w}_i \hat{F}_{n,-i}(t | X_i) \right|. \quad (15)$$

When an independent test set is available (as in our synthetic benchmarks), we also report direct test-set versions of these metrics; see Appendix E.4.

Remark 4.1. Calibration alone does not guarantee useful uncertainty quantification. A well-calibrated predictive distribution can be overly diffuse. Proper scoring rules assess calibration and sharpness jointly (see Appendix C.1).

4.3. Calibration below a Threshold in BO

At iteration n , EI depends on the predictive lower tail below the current best value m_n , through $\hat{F}_n(m_n | x)$ and the restriction of $\hat{F}_n(\cdot | x)$ to $(-\infty, m_n]$. However, calibration at level m_n cannot be assessed from \mathcal{D}_n : by definition, no observation satisfies $f(X_i) < m_n$. We therefore impose calibration below a higher threshold t_n , chosen from the empirical δ -quantile $q_{\delta,n}$ of $(f(X_1), \dots, f(X_n))$ for some $\delta \in (0, 1]$. In the BO algorithm, this threshold can be kept fixed when too few observations fall below the new quantile.

A formal consistency statement showing that occurrence calibration at m_n forces the average predicted improvement probability to vanish as m_n approaches the optimum is given in Appendix D.

5. A Goal-Oriented Calibration Method

5.1. Description of the Method

In this section, we introduce a procedure to select the parameters β and λ of the GN predictive model. We target thresholded μ -calibration below a fixed threshold t , assessed via the truncated CDF $\hat{F}_{n,t}$ on $\{f(X) \leq t\}$, and occurrence calibration at t , assessed by matching p_t with $\mathbb{E}_n[\hat{F}_n(t | X)]$. Following Pion & Vazquez (2025), we fix $l = 0$, so that calibration changes the shape of the predictive distribution without shifting its mean away from the GP mean f_n . Accordingly, we write $\hat{F}_n^{\beta,\lambda}(\cdot | x)$ instead of $\hat{F}_n^{\beta,0,\lambda}(\cdot | x)$.

Parameter selection criterion. Let $U_t^{\beta,\lambda}$ be the μ -tPIT associated with the truncated predictive CDF $\hat{F}_{n,t}^{\beta,\lambda}(\cdot | X)$. Thresholded μ -probabilistic calibration below t is equivalent to

$$\mathbb{P}_n \left(U_t^{\beta,\lambda} \leq u \mid f(X) \leq t \right) = u, \quad u \in [0, 1]. \quad (16)$$

To incorporate occurrence calibration at t , define the occurrence ratio

$$\kappa_t^{\beta,\lambda} = \frac{\mathbb{E}_n \left[\hat{F}_n^{\beta,\lambda}(t | X) \right]}{p_t}. \quad (17)$$

The numerator is the μ -average predicted probability of $\{f(X) \leq t\}$, while the denominator is the μ -probability of $\{f(X) \leq t\}$, so $\kappa_t^{\beta,\lambda} = 1$ is equivalent to occurrence calibration at t . Note that $\kappa_t^{\beta,\lambda} > 1$ indicates an overestimation of p_t and $\kappa_t^{\beta,\lambda} < 1$ an underestimation.

We compare $u \mapsto \mathbb{P}_n(U_t^{\beta,\lambda} \leq u \mid f(X) \leq t)$ to $u \mapsto$

u $\kappa_t^{\beta, \lambda}$ and define

$$J(\beta, \lambda) = \sup_{u \in [0, 1]} \left| \mathbb{P}_n \left(U_t^{\beta, \lambda} \leq u \mid f(X) \leq t \right) - u \kappa_t^{\beta, \lambda} \right|. \quad (18)$$

By construction, $J(\beta, \lambda) = 0$ when $\hat{F}_n^{\beta, \lambda}$ is μ -probabilistically calibrated below t and occurrence-calibrated at t . When $\kappa_t^{\beta, \lambda} = 1$, $J(\beta, \lambda)$ reduces to the tKS-PIT metric. Appendix F.2 reports alternative parameter selection criteria. We use J in the experiments.

LOO approximation. The criterion $J(\beta, \lambda)$ involves μ -expectations and the excursion probability p_t , which are unknown given only \mathcal{D}_n . We use a weighted leave-one-out (LOO) approximation. Let $G_{t,n}^{\text{LOO},w}(u; \beta, \lambda)$ be defined by (13), with $\hat{F}_{n,-i}^{\beta, \lambda}(\cdot \mid x)$ replaced by $\hat{F}_{n,-i}^{\beta, \lambda}(\cdot \mid X_i)$. Define

$$\hat{\kappa}_{t,n}^{\beta, \lambda} = \frac{\sum_{i=1}^n \tilde{w}_i \hat{F}_{n,-i}^{\beta, \lambda}(t \mid X_i)}{\hat{p}_{t,n}^w}, \quad (19)$$

assuming $\hat{p}_{t,n}^w > 0$. The resulting approximation of (18) is

$$J_{t,n}^{\text{LOO},w}(\beta, \lambda) = \sup_{u \in [0, 1]} \left| G_{t,n}^{\text{LOO},w}(u; \beta, \lambda) - u \hat{\kappa}_{t,n}^{\beta, \lambda} \right|. \quad (20)$$

The parameters β and λ are selected by solving

$$(\beta^*, \lambda^*) = \arg \min_{(\beta, \lambda) \in [\beta_0, \beta_1] \times [\lambda_0, \lambda_1]} J_{t,n}^{\text{LOO},w}(\beta, \lambda), \quad (21)$$

where $0 < \lambda_0 < \lambda_1$ and $0 < \beta_0 < \beta_1$. We refer to the method as *calibrated prediction below t for GPs* (TCGP).

The complete TCGP procedure, including its integration into BO, is described in Appendix E.3.

5.2. EI with TCGP

Section 3 defined EI and the BO loop. We now describe the EI algorithm obtained by using TCGP predictive distributions.

Choice of the threshold. The objective is to obtain predictive distributions that are well calibrated below the current best value m_n . Calibrating at level m_n is not feasible from \mathcal{D}_n , since no observation satisfies $Z_i < m_n$ by definition. We therefore calibrate below a higher threshold t_n chosen in the lower tail of the observed responses. Let $q_{\delta, n}$ be the empirical δ -quantile of (Z_1, \dots, Z_n) . At the initial iteration, we set $t_{n_0} = q_{\delta, n_0}$. We use $q_{\delta, n}$ as the candidate threshold when $\hat{p}_{q_{\delta, n}, n}^w \geq p_{\min}$, in which case $t_n = q_{\delta, n}$. If not, we keep the previous threshold. Here, p_{\min} is the minimum estimated excursion probability below a candidate threshold that we allow. This avoids calibrating on too few points when the design concentrates near a minimizer and the lower-tail excursion probability becomes small.

Predictive distribution and EI. Fix (β, λ) . Conditional on \mathcal{D}_n and for $x \in \mathbb{X}$, TCGP uses the predictive CDF $\hat{F}_n^{\beta, \lambda}(\cdot \mid x)$ defined in (3). Let $Z_{n,x}$ be a predictive random variable with this CDF. With the GN model,

$$Z_{n,x} \sim \mathcal{GN}(\beta, f_n(x), \lambda \sigma_n(x)), \quad (22)$$

with the convention that $Z_{n,x} = f_n(x)$ when $\sigma_n(x) = 0$.

The EI criterion induced by $\hat{F}_n^{\beta, \lambda}(\cdot \mid x)$ is

$$\rho_n(x) = \mathbb{E}[(m_n - Z_{n,x})_+ \mid \mathcal{D}_n], \quad (23)$$

where the expectation is taken with respect to the predictive distribution of $Z_{n,x}$ conditional on \mathcal{D}_n . Proposition 5.1 yields the closed form

$$\rho_n(x) = \gamma(m_n - f_n(x), \lambda \sigma_n(x), \beta), \quad (24)$$

where γ is defined in (26).

Proposition 5.1. *If $Z \sim \mathcal{GN}(\beta, l, \lambda)$, then for any $a \in \mathbb{R}$,*

$$\mathbb{E}[(a - Z)_+] = \gamma(a - l, \lambda, \beta), \quad (25)$$

where, for $\lambda > 0$,

$$\gamma(z, \lambda, \beta) = z \Theta_\beta \left(\frac{z}{\lambda} \right) + \frac{\lambda}{2\Gamma(1/\beta)} \Gamma \left(\frac{2}{\beta}, \left| \frac{z}{\lambda} \right|^\beta \right), \quad (26)$$

and $\gamma(z, 0, \beta) = \max(z, 0)$. Here Θ_β denotes the CDF of $\mathcal{GN}(\beta, 0, 1)$ and $\Gamma(\cdot, \cdot)$ is the upper incomplete gamma function. For $\lambda > 0$, $\gamma(\cdot, \lambda, \beta)$ is continuous and satisfies $\gamma(z, \lambda, \beta) > 0$ for all $z \in \mathbb{R}$.

Proof. See Appendix B.1. \square

Remark 5.2. For $\beta = 2$, the GN distribution coincides with a Gaussian distribution, and (26) reduces to the standard EI expression; see Appendix B.2.

BO update. At iteration n , we set $t = t_n$ and obtain (β_n, λ_n) by solving (21). The next evaluation point is selected as

$$X_{n+1} \in \arg \max_{x \in \mathbb{X}} \rho_n(x). \quad (27)$$

Additional implementation details are given in Appendix E.3.

5.3. Convergence of EI with TCGP and Fixed GP Hyperparameters

We prove a convergence result for EI when predictive distributions are obtained with TCGP from a zero-mean GP model with fixed covariance kernel k . This is a sanity check: with fixed hyperparameters and bounded TCGP parameters, EI still produces a dense sequence of evaluation points in \mathbb{X} . Proposition 5.3 extends the exploration result of Vazquez

& Bect (2010) by replacing the Gaussian predictive distribution with the GN family, with parameters (β_n, λ_n) constrained to a compact set.

We assume that k satisfies the no-empty ball (NEB) property (Vazquez & Bect, 2010): for any sequence $(X_n)_{n \geq 1}$ in \mathbb{X} and any $x \in \mathbb{X}$, x is an adherent point of $\{X_n : n \geq 1\}$ iff $\sigma_n^2(x) \rightarrow 0$ as $n \rightarrow \infty$.

Proposition 5.3. *Assume that \mathbb{X} is compact and that k is continuous, stationary, strictly positive definite, and satisfies the NEB property. Let \mathcal{H} be the associated RKHS and assume $f \in \mathcal{H}$. Let f_n and σ_n be the zero-mean noiseless kernel interpolant and kriging standard deviation constructed from \mathcal{D}_n . Assume that there exists $M \geq 1$ such that for all $n \geq M$,*

$$(\beta_n, \lambda_n) \in [\beta_0, \beta_1] \times [\lambda_0, \lambda_1],$$

with $0 < \beta_0 < \beta_1$ and $0 < \lambda_0 < \lambda_1$. Let $(X_n)_{n \geq 1}$ be generated by EI, that is

$$X_{n+1} \in \arg \max_{x \in \mathbb{X}} \rho_n(x),$$

where ρ_n is EI computed from the TCGP predictive CDFs with parameters (β_n, λ_n) . Then (X_n) is dense in \mathbb{X} .

The maximizer exists because f_n , σ_n , and γ are continuous, so ρ_n is continuous on the compact set \mathbb{X} .

Proof. See Appendix B.3. \square

Proposition 5.3 implies that (X_n) intersects every nonempty open subset of \mathbb{X} . Since f is continuous on the compact set \mathbb{X} , for any global minimizer $x^* \in \arg \min_{x \in \mathbb{X}} f(x)$ there exists a subsequence $(X_{n_j})_j$ such that $X_{n_j} \rightarrow x^*$, hence $m_n \rightarrow \min_{x \in \mathbb{X}} f(x)$.

Remark 5.4. In practice, GP hyperparameters are re-estimated at each iteration. Extending Proposition 5.3 to sequential hyperparameter selection is nontrivial (see, e.g., Bull, 2011) and left for future work.

6. Experiments

6.1. Experimental Setup

We study how calibration below a threshold affects BO. We report results for variants targeting occurrence calibration, thresholded μ -calibration, or both, and we compare TCGP with REGP (relaxed interpolation above t_n), BCRGP with density-ratio reweighting (Appendix E.5) for calibration over \mathbb{X} , and the online conformal recalibration method of Deshpande et al. (2024) based on the quantile pinball loss (onGP). For REGP, we use $\delta = 0.25$, and for TCGP, $\delta = 0.05$ (see also Appendices F.3 and F.4). We fix $p_{\min} = 0.015$. Additional diagnostics at t_n and at the current best value m_n are reported in Appendix F.5.

All methods use a GP model with constant mean and an anisotropic Matérn kernel (Appendix E.1), with hyperparameters selected by maximum likelihood at each iteration. Experiments are implemented with `gppmp` (Vazquez, 2026). The benchmark uses standard deterministic test functions (Appendix E.7). Each run starts from an initial design of size $n_0 = 10d$ drawn uniformly on \mathbb{X} , followed by EI-based BO iterations. EI is maximized using a sequential Monte Carlo procedure available in `gppmp` (Appendix E.2). For each test function, we generate 100 independent initial datasets.

BO performance is summarized by the excursion probability below the current best value m_n : for each run and each iteration n , we consider $p_{m_n} = \mathbb{P}(f(X) \leq m_n)$, $X \sim \mathcal{U}(\mathbb{X})$, and estimate p_{m_n} by subset simulation (Bect et al., 2017) as the main performance metric. We then report, as a function of n , the median and the 10% and 90% quantiles of p_{m_n} across the 100 runs.

6.2. Thresholded and Occurrence Calibration: Empirical Comparison

We compare the roles of occurrence calibration, thresholded tail-rank calibration, and their combination in BO. We compare a standard GP model with three TCGP variants. The first variant, TCGP-thres, selects (β, λ) by minimizing the weighted LOO tKS–PIT, targeting thresholded μ -calibration. The second, TCGP-occ, minimizes the weighted LOO occurrence discrepancy r_t . The joint variant, TCGP, uses the selection criterion of Section 5.

At each BO iteration, we report BO performance and test-set calibration metrics evaluated at the current best value m_n : twCRPS, tKS–PIT below m_n , and r_t (details about the metrics provided in Appendices C.2 and E.4). The twCRPS and r_t use 1000 test points sampled in \mathbb{X} , while tKS–PIT uses 900 test points conditioned on $f(x) \leq m_n$.

Figure 2 reports results for Ackley ($d = 4$) and Goldstein–Price. On Ackley, TCGP-thres reduces tKS–PIT but does not improve r_t or twCRPS, and BO progresses more slowly. TCGP-occ substantially reduces r_t and improves optimization performance despite a degraded tKS–PIT, suggesting that correcting tail mass can matter more for EI than improving tail ranks alone. Neither single-component variant improves upon the standard GP model. The joint method TCGP performs best. It rapidly reduces r_t and improves tKS–PIT early, leading to faster decreases of m_n . As the design concentrates near a minimizer and m_n approaches the optimum, calibration below m_n relies on fewer test points and optimization slows down.

On Goldstein–Price, all TCGP-based variants improve over the GP and quickly reduce twCRPS and r_t . TCGP and TCGP-occ behave similarly and outperform TCGP-thres, again indicating that occurrence calibration has a stronger

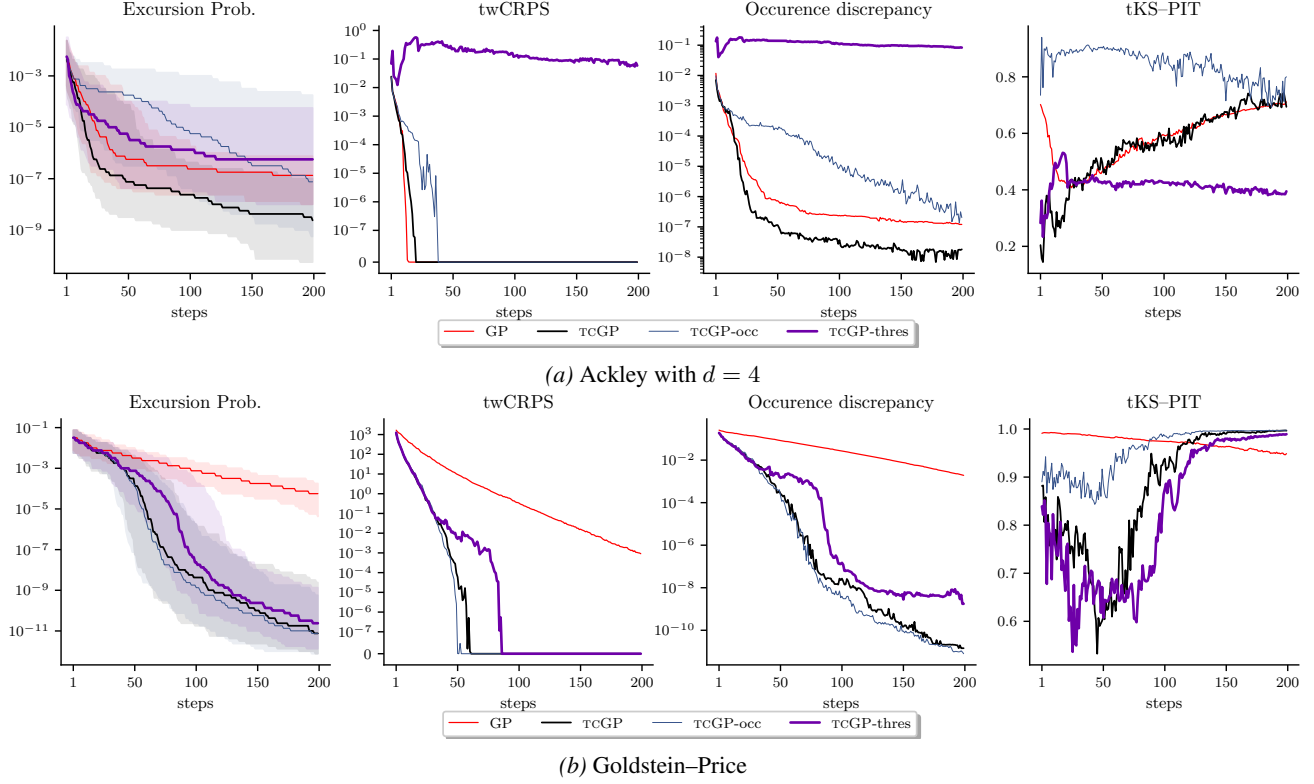


Figure 2. BO performance and calibration metrics. From left to right: median and 10%/90% quantiles across runs of the estimated excursion probability $p_{m_n} = \mathbb{P}(f(X) \leq m_n)$ with $X \sim \mathcal{U}(\mathbb{X})$; median twCRPS; median occurrence discrepancy r_t ; and median tKS-PIT. Calibration metrics are evaluated on a test set at the current best value m_n . Results are shown for a standard GP and three TCGP variants using J , tKS-PIT, or r_t as the parameter selection criterion ($\delta = 0.05$).

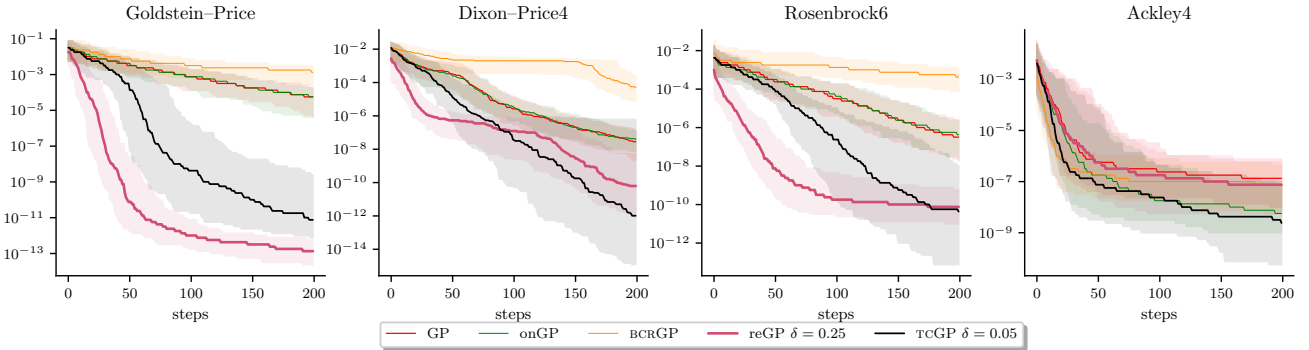


Figure 3. BO performance summarized by the excursion probability below the current best value. For each run and iteration n , we estimate $p_{m_n} = \mathbb{P}(f(X) \leq m_n)$ with $X \sim \mathcal{U}(\mathbb{X})$, and report the median and 10%/90% quantiles of p_{m_n} across runs for Goldstein-Price, Dixon-Price ($d = 4$), Rosenbrock ($d = 6$), and Ackley ($d = 4$). Methods: GP, BCRGP, onGP, REGP ($\delta = 0.25$), TCGP ($\delta = 0.05$).

effect on EI-driven BO than thresholded μ -calibration alone.

Overall, these results suggest that accurate occurrence calibration at m_n is often important for BO, with thresholded μ -calibration providing an additional gain. Focusing only on the thresholded notion can yield poor optimization performance because it does not control systematic over- or under-estimation of improvement probabilities over \mathbb{X} .

6.3. Comparison across Methods

We compare EI-based BO with a standard GP model, REGP, TCGP, onGP, and BCRGP on four test functions: Ackley ($d = 4$), Dixon-Price ($d = 4$), Rosenbrock ($d = 6$), and Goldstein-Price. Figure 3 reports the evolution of the median and the 10%/90% quantiles of $p_{m_n} = \mathbb{P}(f(X) \leq m_n)$, where m_n denotes the best observed value so far. To complement these results, Appendix F.6 reports additional EI ex-

periments on Ackley, Crossintray, Dixon–Price, Goldstein–Price, Hartmann, Michalewicz, Rosenbrock, Shekel, and Perm, in dimensions ranging from $d = 2$ to $d = 20$, together with additional results for the *upper confidence bound* (UCB) criterion.

On Goldstein–Price, Dixon–Price, and Rosenbrock, REGP and TCGP improve over the standard GP model, with REGP performing best on these smoother objectives. On Ackley, TCGP provides the largest gains.

BCRGP does not consistently improve over the standard GP model, suggesting that global calibration over \mathbb{X} alone is not sufficient to improve EI. The online conformal method onGP is close to the standard GP model on these noiseless benchmarks, except on Ackley.

Appendix F.6 reports similar qualitative patterns for both EI and UCB sampling criteria. On functions where the standard GP model is already competitive, such as Ackley, Michalewicz, or Shekel, TCGP and REGP provide only small improvements. In these cases, calibration has little effect on BO performance.

Calibrating below a low threshold improves BO in these settings. REGP and TCGP show complementary strengths, with REGP incurring a larger computational overhead than TCGP (Appendix F.1).

7. Discussion and Limitations

We introduced a goal-oriented calibration framework for Bayesian optimization, built on two design-marginal notions: occurrence calibration at a threshold and thresholded μ -calibration below that threshold. The ablation study indicates that the joint criterion is more consistent than variants targeting only one of the two notions. In the deterministic GP-based experiments, TCGP changes the behavior of EI and UCB and improves performance on several benchmarks, while remaining cheaper to train than REGP.

The study is restricted to the exact-evaluation setting. In noisy problems, the latent objective is no longer directly observed, so the calibration targets considered here are not directly accessible from the data and would need to be re-defined. The experiments are also mostly low-to-moderate dimensional, where the weighted leave-one-out estimates are more stable. Future work can study extensions to noisy BO and to higher-dimensional problems.

Acknowledgements

This work was supported by TRANSVALOR S.A. through a CIFRE PhD agreement. We thank TRANSVALOR S.A. for its support.

Impact Statement

Improved lower-tail calibration can reduce the number of expensive evaluations required in Bayesian optimization. The impact is application-dependent, since the same methodology can be used for beneficial or harmful optimization goals.

Conflict of Interest Disclosure

Aurélien Pion is affiliated with TRANSVALOR S.A. The article does not evaluate a proprietary product or model developed by TRANSVALOR S.A. The authors declare no other financial conflicts of interest.

References

- Allen, S., Bhend, J., Martius, O., and Ziegel, J. Weighted verification tools to evaluate univariate and multivariate probabilistic forecasts for high-impact weather events. *Weather and Forecasting*, 38(3):499 – 516, 2023.
- Allen, S., Koh, J., Segers, J., and Ziegel, J. Tail calibration of probabilistic forecasts. *J. Amer. Statist. Assoc.*, 120(552):2796–2808, 2025.
- Auer, P., Cesa-Bianchi, N., and Fischer, P. Finite-time analysis of the multiarmed bandit problem. *Mach. Learn.*, 47:235–256, 2002.
- Bect, J., Li, L., and Vazquez, E. Bayesian subset simulation. *SIAM/ASA Journal on Uncertainty Quantification*, 5(1): 762–786, 2017.
- Bogunovic, I. and Krause, A. Misspecified Gaussian process bandit optimization. In Ranzato, M., Beygelzimer, A., Dauphin, Y., Liang, P., and Vaughan, J. W. (eds.), *Adv. Neural Inf. Process. Syst.*, volume 34, pp. 3004–3015. Curran Associates, Inc., 2021.
- Bull, A. D. Convergence rates of efficient global optimization algorithms. *J. Mach. Learn. Res.*, 12(88):2879–2904, 2011.
- Chu, W. and Ghahramani, Z. Gaussian processes for ordinal regression. *J. Mach. Learn. Res.*, 6(35):1019–1041, 2005.
- Deshpande, S., Marx, C., and Kuleshov, V. Online calibrated and conformal prediction improves Bayesian optimization. In Dasgupta, S., Mandt, S., and Li, Y. (eds.), *Proceedings of The 27th International Conference on Artificial Intelligence and Statistics*, volume 238 of *Proc. Mach. Learn. Res.*, pp. 1450–1458. PMLR, 02–04 May 2024.
- Feliot, P., Bect, J., and Vazquez, E. A Bayesian approach to constrained single- and multi-objective optimization. *J. Global Optim.*, 67(1-2):97–133, April 2016.

- Forrester, A. I. J., Sóbester, A., and Keane, A. J. *Engineering Design via Surrogate Modelling: A Practical Guide*. John Wiley & Sons, 2008.
- Friedli, L., Gautier, A., Broccard, A., and Ginsbourger, D. CRPS-based targeted sequential design with application in chemical space, 2025. URL <https://arxiv.org/abs/2503.11250>.
- Gneiting, T. and Resin, J. Regression diagnostics meets forecast evaluation: conditional calibration, reliability diagrams, and coefficient of determination. *Electron. J. Stat.*, 17(2), January 2023.
- Gneiting, T., Balabdaoui, F., and Raftery, A. E. Probabilistic forecasts, calibration and sharpness. *J. R. Stat. Soc. Ser. B Stat. Methodol.*, 69(2):243–268, 2007.
- Gneiting, T. G. and Raftery, A. E. Strictly proper scoring rules, prediction, and estimation. *J. Am. Stat. Assoc.*, 102(477):359–378, 2007.
- Guo, Z., Ong, Y. S., and Liu, H. Calibrated and recalibrated expected improvements for Bayesian optimization. *Struct. Multidiscip. Optim.*, 64:3549–3567, 2021.
- Jin, Y. and Ren, Z. Confidence on the focal: conformal prediction with selection-conditional coverage. *J. R. Stat. Soc. Ser. B. Stat. Methodol.*, 87(4):1239–1259, 04 2025.
- Jones, D., Schonlau, M., and Welch, W. Efficient global optimization of expensive black-box functions. *J. Global Optim.*, 13:455–492, 12 1998.
- Kim, D., Zecchin, M., Park, S., Kang, J., and Simeone, O. Robust Bayesian optimization via localized online conformal prediction. *IEEE Trans. Signal Process.*, 73: 2039–2052, 2025.
- Lai, T. L. and Robbins, H. Asymptotically efficient adaptive allocation rules. *Adv. Appl. Math.*, 6(1):4–22, 1985.
- Matheson, J. E. and Winkler, R. L. Scoring rules for continuous probability distributions. *Manag. Sci.*, 22(10): 1087–1096, 1976.
- Meeker, W. Q., Hahn, G. J., and Escobar, L. A. *Statistical Intervals: A Guide for Practitioners and Researchers*. John Wiley & Sons, Hoboken, New Jersey, second edition, 2017. ISBN 978-0-471-68717-7.
- Mockus, J., Tiesis, V., and Zilinskas, A. The application of Bayesian methods for seeking the extremum. In Dixon, L. C. W. and Szegö, G. P. (eds.), *Towards Global Optimization*, volume 2, pp. 117–129. North-Holland, Amsterdam, 1978.
- Nadarajah, S. A generalized normal distribution. *J. Appl. Stat.*, 32(7):685–694, 2005.
- Neiswanger, W. and Ramdas, A. Uncertainty quantification using martingales for misspecified Gaussian processes. In Feldman, V., Ligett, K., and Sabato, S. (eds.), *Proceedings of the 32nd International Conference on Algorithmic Learning Theory*, volume 132 of *Proc. Mach. Learn. Res.*, pp. 963–982. PMLR, 16–19 Mar 2021.
- Nelder, J. A. and Mead, R. A simplex method for function minimization. *The Computer Journal*, 7(4):308–313, 01 1965.
- Petit, S. J., Bect, J., and Vazquez, E. Relaxed Gaussian process interpolation: a goal-oriented approach to Bayesian optimization. *Journal of Machine Learning Research*, 26(195):1–70, 2025.
- Picheny, V., Vakili, S., and Artemev, A. Ordinal Bayesian optimisation, 2019. URL <https://arxiv.org/abs/1912.02493>.
- Picheny, V., Moss, H., Torossian, L., and Durrande, N. Bayesian quantile and expectile optimisation. In Cussens, J. and Zhang, K. (eds.), *Proceedings of the Thirty-Eighth Conference on Uncertainty in Artificial Intelligence*, volume 180 of *Proc. Mach. Learn. Res.*, pp. 1623–1633. PMLR, 01–05 Aug 2022.
- Pion, A. and Vazquez, E. Design-marginal calibration of Gaussian process predictive distributions: Bayesian and conformal approaches, 2025. URL <https://arxiv.org/abs/2512.05611>.
- Sahoo, R., Zhao, S., Chen, A., and Ermon, S. Reliable decisions with threshold calibration. In Ranzato, M., Beygelzimer, A., Dauphin, Y., Liang, P., and Vaughan, J. W. (eds.), *Adv. Neural Inf. Process. Syst.*, volume 34, pp. 1831–1844. Curran Associates, Inc., 2021.
- Schonlau, M. and Welch, W. J. Global optimization with nonparametric function fitting. In *Proceedings of the ASA, Section on Physical and Engineering Sciences*, pp. 183–186. Amer. Statist. Assoc., 1996.
- SciPy Developers. *SciPy Project*, 2026. URL <https://docs.scipy.org/doc/scipy/reference/generated/scipy.stats.gennorm.html>. SciPy API Reference, accessed 2026-01.
- Scott, D. W. *Multivariate Density Estimation: Theory, Practice, and Visualization*. John Wiley & Sons, New York, 1992.
- Shimodaira, H. Improving predictive inference under covariate shift by weighting the log-likelihood function. *J. Statist. Plann. Inference*, 90(2):227–244, 2000.
- Srinivas, N., Krause, A., Kakade, S. M., and Seeger, M. Gaussian process optimization in the bandit setting: No

- regret and experimental design. In *Proc. 27th International Conference on Machine Learning (ICML 2010)*, pp. 1015–1022, 2010.
- Stanton, S., Maddox, W., and Wilson, A. G. Bayesian optimization with conformal prediction sets. In Ruiz, F., Dy, J., and van de Meent, J. W. (eds.), *Proceedings of The 26th International Conference on Artificial Intelligence and Statistics*, volume 206 of *Proc. Mach. Learn. Res.*, pp. 959–986. PMLR, 25–27 Apr 2023.
- Stein, M. L. *Interpolation of Spatial Data: Some Theory for Kriging*. Springer Ser. Stat. Springer New York, 1999.
- Surjanovic, S. and Bingham, D. Virtual library of simulation experiments: Test functions and datasets, 2013. URL <https://www.sfu.ca/~ssurjano/>. Accessed November 2025.
- Tom, G., Lo, S., Corapi, S., Aspuru-Guzik, A., and Sanchez-Lengeling, B. Ranking over regression for Bayesian optimization and molecule selection. *APL Machine Learning*, 3(3):036113, 08 2025.
- Tuo, R. and Wang, W. Uncertainty quantification for Bayesian optimization. In Camps-Valls, G., Ruiz, F. J. R., and Valera, I. (eds.), *Proceedings of the 25th International Conference on Artificial Intelligence and Statistics (AISTATS)*, volume 151 of *Proc. Mach. Learn. Res.*, pp. 2862–2884. PMLR, 2022.
- Vazquez, E. Gpmp: the Gaussian process micro package, 2026. URL <https://github.com/gpmp-dev/gpmp>.
- Vazquez, E. and Bect, J. Convergence properties of the expected improvement algorithm with fixed mean and covariance functions. *J. Statist. Plann. Inference*, 140: 3088–3095, 11 2010.
- Villemonteix, J., Vazquez, E., and Walter, E. An informational approach to the global optimization of expensive-to-evaluate functions. *J. Global Optim.*, 44(4):509–534, 2009.
- Vovk, V., Gammerman, A., and Shafer, G. *Algorithmic Learning in a Random World*. Springer, 2005.
- Vovk, V., Shen, J., Manokhin, V., and Xie, M. Nonparametric predictive distributions based on conformal prediction. *Mach. Learn.*, 108(3):445–474, 2019.
- Zhang, Y. and Candès, E. J. Posterior conformal prediction, 2024. URL <https://arxiv.org/abs/2409.19712>.

Appendices

The appendix is organized as follows. Appendix [A](#) recalls the generalized normal distribution. Appendix [B](#) gathers the proofs of the main results. Appendix [C](#) briefly reviews scoring rules. Appendix [D](#) presents the consistency statement discussed in Section 4.3. Appendix [E](#) provides implementation details, and Appendix [F](#) reports additional experimental results.

A. Generalized Normal Distribution

The generalized normal distribution $\mathcal{GN}(\beta, l, \lambda)$ is a three-parameter family on \mathbb{R} , with shape parameter $\beta > 0$, location parameter $l \in \mathbb{R}$, and scale parameter $\lambda > 0$. Its density is

$$g(z) = \frac{\beta}{2\Gamma(1/\beta)\lambda} \exp\left(-\left(\frac{|z-l|}{\lambda}\right)^\beta\right), \quad z \in \mathbb{R}. \quad (28)$$

It is symmetric about l . The mean is $\mathbb{E}[Z] = l$ and the variance is

$$\text{var}(Z) = \lambda^2 \frac{\Gamma(3/\beta)}{\Gamma(1/\beta)}. \quad (29)$$

The parameter β controls tail decay: $\beta = 2$ yields a Gaussian distribution, $\beta < 2$ corresponds to heavier tails, and $\beta > 2$ to lighter tails. In particular,

$$\mathcal{GN}(2, l, \lambda) = \mathcal{N}\left(l, \frac{\lambda^2}{2}\right), \quad (30)$$

since $\Gamma(3/2)/\Gamma(1/2) = 1/2$.

The cumulative distribution function can be written using the lower incomplete gamma function

$$\gamma(a, x) = \int_0^x t^{a-1} e^{-t} dt. \quad (31)$$

For $z \in \mathbb{R}$, the CDF $\Theta_{\beta, l, \lambda}$ of $\mathcal{GN}(\beta, l, \lambda)$ may be written as

$$\Theta_{\beta, l, \lambda}(z) = \mathbb{P}(Z \leq z) = \begin{cases} \frac{1}{2} - \frac{1}{2\Gamma(1/\beta)} \gamma\left(\frac{1}{\beta}, \left(\frac{l-z}{\lambda}\right)^\beta\right), & z \leq l, \\ \frac{1}{2} + \frac{1}{2\Gamma(1/\beta)} \gamma\left(\frac{1}{\beta}, \left(\frac{z-l}{\lambda}\right)^\beta\right), & z \geq l. \end{cases} \quad (32)$$

We also write $\Theta_\beta := \Theta_{\beta, 0, 1}$.

Further properties are given in [Nadarajah \(2005\)](#). The distribution $\mathcal{GN}(\beta, l, \lambda)$ is available in SciPy as `scipy.stats.gennorm`; see [SciPy Developers \(2026\)](#).

B. Proofs

B.1. Proof of Proposition 5.1

Proof. Let $\beta > 0$ and $\lambda > 0$. Write $Z = l + \lambda T$ with $T \sim \mathcal{GN}(\beta, 0, 1)$, whose density is

$$g_\beta(t) = \frac{\beta}{2\Gamma(1/\beta)} \exp(-|t|^\beta). \quad (33)$$

Set $z = a - l$ and $s = z/\lambda$. Then

$$\mathbb{E}[(a - Z)_+] = \mathbb{E}[(z - \lambda T)_+] = \lambda \mathbb{E}[(s - T)_+] = \lambda \int_{-\infty}^s (s - t) g_\beta(t) dt. \quad (34)$$

Therefore,

$$\mathbb{E}[(a - Z)_+] = \lambda \left(s \Theta_\beta(s) - \int_{-\infty}^s t g_\beta(t) dt \right). \quad (35)$$

It remains to compute $\int_{-\infty}^s t g_\beta(t) dt$. Since $t \mapsto t \exp(-|t|^\beta)$ is odd, for any $s \in \mathbb{R}$,

$$\int_{-\infty}^s t \exp(-|t|^\beta) dt = - \int_{|s|}^{\infty} u \exp(-u^\beta) du. \quad (36)$$

By the change of variables $y = u^\beta$,

$$\int_{|s|}^{\infty} u \exp(-u^\beta) du = \frac{1}{\beta} \int_{|s|^\beta}^{\infty} y^{2/\beta-1} \exp(-y) dy = \frac{1}{\beta} \Gamma\left(\frac{2}{\beta}, |s|^\beta\right). \quad (37)$$

Hence,

$$\int_{-\infty}^s t g_\beta(t) dt = \frac{\beta}{2\Gamma(1/\beta)} \int_{-\infty}^s t \exp(-|t|^\beta) dt = -\frac{1}{2\Gamma(1/\beta)} \Gamma\left(\frac{2}{\beta}, |s|^\beta\right). \quad (38)$$

Substituting back yields

$$\mathbb{E}[(a - Z)_+] = \lambda \left(s \Theta_\beta(s) + \frac{1}{2\Gamma(1/\beta)} \Gamma\left(\frac{2}{\beta}, |s|^\beta\right) \right) = z \Theta_\beta\left(\frac{z}{\lambda}\right) + \frac{\lambda}{2\Gamma(1/\beta)} \Gamma\left(\frac{2}{\beta}, \left|\frac{z}{\lambda}\right|^\beta\right). \quad (39)$$

This is (26).

For $\lambda = 0$, $Z = l$ almost surely, so $\mathbb{E}[(a - Z)_+] = \max(a - l, 0)$, which defines $\gamma(z, 0, \beta)$. Continuity at $\lambda = 0$ follows by considering three cases. If $z > 0$, then $\Theta_\beta(z/\lambda) \rightarrow 1$ and the incomplete-gamma term vanishes. If $z < 0$, then $\Theta_\beta(z/\lambda) \rightarrow 0$ and the same incomplete-gamma term vanishes. If $z = 0$, the first term is identically zero and the second term is $\lambda\Gamma(2/\beta)/(2\Gamma(1/\beta))$, hence converges to zero. Strict positivity for $\lambda > 0$ holds because Z has a continuous density that is strictly positive on \mathbb{R} , hence $\mathbb{P}(Z < a) > 0$ for any finite a , and $(a - Z)_+ > 0$ on $\{Z < a\}$. \square

B.2. Connection between EI in the Gaussian Case and the Generalized Normal Model

For $\beta = 2$, the generalized normal distribution coincides with a Gaussian:

$$\mathcal{GN}(2, l, \lambda) = \mathcal{N}\left(l, \frac{\lambda^2}{2}\right). \quad (40)$$

Let $\sigma = \lambda/\sqrt{2}$ and $\tau = (a - l)/\sigma$. For $\beta = 2$ we have $\Theta_2(s) = \Phi(\sqrt{2}s)$, and $\Gamma(1, x) = \exp(-x)$. Substituting into (26) yields

$$\gamma(a - l, \lambda, 2) = (a - l)\Phi(\tau) + \sigma\varphi(\tau), \quad (41)$$

where Φ and φ denote the CDF and PDF of $\mathcal{N}(0, 1)$. This is the usual EI formula for a Gaussian predictive distribution with mean l and standard deviation σ .

B.3. Proof of Proposition 5.3

Recall that, at iteration n , EI with TCGP is

$$\rho_n(x) = \gamma(m_n - f_n(x), \lambda_n \sigma_n(x), \beta_n), \quad m_n = \min_{1 \leq i \leq n} f(X_i), \quad (42)$$

and we set

$$\nu_n(f) = \max_{x \in \mathbb{X}} \rho_n(x) = \rho_n(X_{n+1}), \quad X_{n+1} \in \arg \max_{x \in \mathbb{X}} \rho_n(x), \quad (43)$$

with $(\beta_n, \lambda_n) \in [\beta_0, \beta_1] \times [\lambda_0, \lambda_1]$ and $\lambda_0 > 0$ for all sufficiently large n .

Lemma B.1. *Let $0 < \beta_0 < \beta_1$. The map $(z, s, \beta) \mapsto \gamma(z, s, \beta)$, with $\gamma(z, 0, \beta) = z_+$, is continuous on compact subsets of $\mathbb{R} \times [0, \infty) \times [\beta_0, \beta_1]$.*

Proof. For $s > 0$, continuity follows from the closed-form expression (26). It remains to check continuity at $s = 0$, uniformly for $\beta \in [\beta_0, \beta_1]$. Let $T_\beta \sim \mathcal{GN}(\beta, 0, 1)$. Since the map $x \mapsto x_+$ is Lipschitz,

$$|\gamma(z, s, \beta) - z_+| = |\mathbb{E}[(z - sT_\beta)_+] - z_+| \leq s \mathbb{E}|T_\beta|. \quad (44)$$

Moreover,

$$\mathbb{E}|T_\beta| = \frac{\Gamma(2/\beta)}{\Gamma(1/\beta)} \quad (45)$$

is bounded on $[\beta_0, \beta_1]$ by continuity. Hence $\gamma(z, s, \beta) \rightarrow z_+$ as $s \downarrow 0$, uniformly for $\beta \in [\beta_0, \beta_1]$. If also $z' \rightarrow z$, then $|z'_+ - z_+| \rightarrow 0$, so continuity holds at $s = 0$ as well. This proves the claim. \square

Lemma B.2. For all $f \in \mathcal{H}$, $\liminf_{n \rightarrow \infty} \nu_n(f) = 0$.

Proof. Fix $f \in \mathcal{H}$. Since \mathbb{X} is compact, (X_n) has a cluster point $\tilde{x} \in \mathbb{X}$ and there exists a strictly increasing map $\phi : \mathbb{N} \rightarrow \mathbb{N}$ such that $X_{\phi(n)} \rightarrow \tilde{x}$. Since k is continuous and \mathbb{X} is compact, every $f \in \mathcal{H}$ is continuous on \mathbb{X} , hence $f(X_{\phi(n)}) \rightarrow f(\tilde{x})$.

By Vazquez & Bect (2010, Prop. 10),

$$f_{\phi(n)-1}(X_{\phi(n)}) \rightarrow f(\tilde{x}), \quad \sigma_{\phi(n)-1}(X_{\phi(n)}) \rightarrow 0. \quad (46)$$

Moreover, since ϕ is increasing,

$$m_{\phi(n)-1} \leq m_{\phi(n-1)} \leq f(X_{\phi(n-1)}) \rightarrow f(\tilde{x}), \quad (47)$$

hence $\limsup_{n \rightarrow \infty} m_{\phi(n)-1} \leq f(\tilde{x})$. Set

$$z_{\phi(n)-1} := m_{\phi(n)-1} - f_{\phi(n)-1}(X_{\phi(n)}). \quad (48)$$

Then $\limsup_{n \rightarrow \infty} z_{\phi(n)-1} \leq 0$. Define also

$$t_{\phi(n)-1} := \lambda_{\phi(n)-1} \sigma_{\phi(n)-1}(X_{\phi(n)}), \quad (49)$$

so that $t_{\phi(n)-1} \rightarrow 0$ since $0 < \lambda_{\phi(n)-1} \leq \lambda_1$.

Fix $\varepsilon > 0$. For n large enough, $z_{\phi(n)-1} \leq \varepsilon$. For $\lambda > 0$, $z \mapsto \gamma(z, \lambda, \beta) = \mathbb{E}[(z - Z)_+]$ is nondecreasing, hence

$$\nu_{\phi(n)-1}(f) = \rho_{\phi(n)-1}(X_{\phi(n)}) \quad (50)$$

$$= \gamma(z_{\phi(n)-1}, t_{\phi(n)-1}, \beta_{\phi(n)-1}) \quad (51)$$

$$\leq \gamma(\varepsilon, t_{\phi(n)-1}, \beta_{\phi(n)-1}). \quad (52)$$

Since $t_{\phi(n)-1} \rightarrow 0$ and, for all large n , $\beta_{\phi(n)-1} \in [\beta_0, \beta_1]$, every subsequence of $\gamma(\varepsilon, t_{\phi(n)-1}, \beta_{\phi(n)-1})$ has a further subsequence along which $\beta_{\phi(n)-1} \rightarrow \bar{\beta} \in [\beta_0, \beta_1]$. Along this further subsequence, Lemma B.1 gives

$$\gamma(\varepsilon, t_{\phi(n)-1}, \beta_{\phi(n)-1}) \longrightarrow \gamma(\varepsilon, 0, \bar{\beta}) = \varepsilon. \quad (53)$$

Thus the full sequence converges to ε . Therefore,

$$\limsup_{n \rightarrow \infty} \nu_{\phi(n)-1}(f) \leq \varepsilon. \quad (54)$$

Since $\varepsilon > 0$ is arbitrary, $\liminf_{n \rightarrow \infty} \nu_n(f) = 0$. \square

Proof of Proposition 5.3. Assume by contradiction that (X_n) is not dense in \mathbb{X} . Then there exists $\tilde{x} \in \mathbb{X}$ such that \tilde{x} is not adherent to $\{X_n : n \geq 1\}$. By the NEB property, $\sigma_n^2(\tilde{x})$ does not converge to 0. Since $(\sigma_n^2(\tilde{x}))_{n \geq 1}$ is nonincreasing, it converges to some $c^2 > 0$, hence $\inf_{n \geq 1} \sigma_n(\tilde{x}) \geq c$.

Since f_n is the \mathcal{H} -projection of f onto the span of kernel sections, $\|f_n\|_{\mathcal{H}} \leq \|f\|_{\mathcal{H}}$, hence

$$|f_n(\tilde{x})| \leq \|f_n\|_{\mathcal{H}} \sqrt{k(\tilde{x}, \tilde{x})} \leq \|f\|_{\mathcal{H}} \sqrt{k(\tilde{x}, \tilde{x})}. \quad (55)$$

Also, (m_n) is bounded because f is continuous on the compact set \mathbb{X} . Therefore, $z_n^* := m_n - f_n(\tilde{x})$ ranges in a compact interval $I \subset \mathbb{R}$ and $\sigma_n(\tilde{x})$ ranges in $[c, \sqrt{k(\tilde{x}, \tilde{x})}]$.

Define

$$\psi(z, \sigma, \beta, \lambda) = \gamma(z, \lambda\sigma, \beta). \quad (56)$$

The map ψ is continuous by Lemma B.1. Consider the compact set

$$K = I \times [c, \sqrt{k(\tilde{x}, \tilde{x})}] \times [\beta_0, \beta_1] \times [\lambda_0, \lambda_1]. \quad (57)$$

Since $\lambda_0 > 0$ and $\gamma(\cdot, \lambda, \beta)$ is strictly positive for $\lambda > 0$, we have $\psi > 0$ on K , hence

$$\eta := \inf_{(z, \sigma, \beta, \lambda) \in K} \psi(z, \sigma, \beta, \lambda) > 0. \quad (58)$$

For all sufficiently large n ,

$$\rho_n(\tilde{x}) = \gamma(z_n^*, \lambda_n \sigma_n(\tilde{x}), \beta_n) \geq \eta. \quad (59)$$

Since X_{n+1} maximizes ρ_n , we obtain

$$\nu_n(f) = \rho_n(X_{n+1}) \geq \rho_n(\tilde{x}) \geq \eta \quad \text{for all sufficiently large } n, \quad (60)$$

which contradicts Lemma B.2. Therefore, (X_n) is dense in \mathbb{X} . \square

C. Scoring Rules

C.1. General Definition

To assess both sharpness and calibration, we use *proper scoring rules* (Gneiting & Raftery, 2007). Scoring rules assign a numerical score $S(\hat{F}, z)$ to a predictive forecast \hat{F} and an outcome $z \in \mathbb{R}$. A scoring rule is *strictly proper* if, for the true distribution F ,

$$\mathbb{E}_{Z \sim F}[S(F, Z)] \leq \mathbb{E}_{Z \sim F}[S(\hat{F}, Z)], \quad (61)$$

with equality if and only if $\hat{F} = F$.

For goal-oriented prediction, Matheson & Winkler (1976) introduces the *weighted continuous ranked probability score* (twCRPS), defined for a *weight* function w , for instance $w(u) = \mathbb{1}\{u \leq t\}$, by

$$S_{\text{twCRPS}}(\hat{F}, z) = \int (\hat{F}(u) - \mathbb{1}\{u \geq z\})^2 w(u) du. \quad (62)$$

For nonconstant weights, twCRPS is a proper weighted score and does not identify the full predictive distribution outside the weighted region.

Given a true CDF F , a forecasted CDF \hat{F} , and a scoring rule S the predictive performance is evaluated using the expected score

$$J_S(\hat{F}) = \mathbb{E}_{Z \sim F}(S(\hat{F}, Z)). \quad (63)$$

An empirical version is given below. In the spatial setting the expected score of the family of predicted forecast CDFs $\hat{F}_n(\cdot | x)$, indexed by $x \in \mathbb{X}$ is given by,

$$J_{S, \mu}(\hat{F}_n) = \mathbb{E}_n \left[S(\hat{F}_n(\cdot | X), f(X)) \right]. \quad (64)$$

C.2. Empirical twCRPS

Let weight function $w : \mathbb{R} \rightarrow \mathbb{R}^+$ and \hat{F} a forecasted CDF. In the following consider the *chaining* function v defined as any function that verifies $v(x') - v(x) = \int_x^{x'} w(u) du$ (see, e.g., Allen et al., 2023). The twCRPS at $z \in \mathbb{R}$ can be rewritten as

$$S_{\text{twCRPS}}(\hat{F}, z) = \mathbb{E}_{\hat{F}} [|v(Y) - v(z)|] - \frac{1}{2} \mathbb{E}_{\hat{F}} [|v(Y) - v(Y')|], \quad (65)$$

where Y and Y' are independent random variables with CDF \hat{F} .

For a threshold $t \in \mathbb{R}$, let $w(z) = \mathbb{1}\{z \leq t\}$, then $v(z) = \min(z, t)$.

For the empirical forecast-observation pair (Z, \hat{F}) and a sample $(Y_\ell)_{\ell=1}^K$ from \hat{F} , the twCRPS at Z can be approximated by the Monte Carlo estimator

$$\hat{S}_{\text{twCRPS},K}(\hat{F}, Z) = \frac{1}{K} \sum_{\ell=1}^K |v(Y_\ell) - v(Z)| - \frac{1}{2K^2} \sum_{\ell=1}^K \sum_{r=1}^K |v(Y_\ell) - v(Y_r)|. \quad (66)$$

For multiple forecast-observation pairs $(Z_i, \hat{F}_i)_{i=1}^m$, the empirical score is

$$\hat{J}_{\text{twCRPS},m} = \frac{1}{m} \sum_{i=1}^m \hat{S}_{\text{twCRPS},K}(\hat{F}_i, Z_i). \quad (67)$$

D. Impact of Calibration at the Current Best Value

This appendix provides the consistency statement mentioned in Section 4.3. It shows that, if one could enforce occurrence calibration at the current best value m_n , then the predicted probability mass below m_n must collapse as m_n approaches the global minimum.

Proposition D.1 (Vanishing tail mass with occurrence calibration at m_n). *Assume that $m_n \xrightarrow{\text{a.s.}} f(x^*)$ for some global minimizer $x^* \in \arg \min_{x \in \mathbb{X}} f(x)$. If \hat{F}_n is occurrence-calibrated at threshold m_n , that is,*

$$\mathbb{E}_n[\hat{F}_n(m_n | X)] = \mathbb{P}_n(f(X) \leq m_n), \quad X \sim \mu, \quad (68)$$

then for every $\varepsilon \in (0, 1]$, we have

$$\limsup_{n \rightarrow \infty} \mathbb{P}_n(\hat{F}_n(m_n | X) > \varepsilon) \leq \varepsilon^{-1} \mu(\{x \in \mathbb{X} : f(x) = f(x^*)\}) \quad \text{a.s.} \quad (69)$$

In particular, if $\mu(\{x \in \mathbb{X} : f(x) = f(x^*)\}) = 0$, then

$$\mathbb{P}_n(\hat{F}_n(m_n | X) > \varepsilon) \rightarrow 0 \quad \text{a.s.} \quad (70)$$

Proof. Fix $\varepsilon \in (0, 1]$ and set $A_n := \{\hat{F}_n(m_n | X) > \varepsilon\}$. By Markov's inequality,

$$\mathbb{P}_n(A_n) \leq \varepsilon^{-1} \mathbb{E}_n[\hat{F}_n(m_n | X)].$$

Using (68), this yields

$$\mathbb{P}_n(\hat{F}_n(m_n | X) > \varepsilon) \leq \varepsilon^{-1} \mathbb{P}_n(f(X) \leq m_n). \quad (71)$$

On any sample path such that $m_n \rightarrow f(x^*)$, we have $f(x) \geq f(x^*)$ for all $x \in \mathbb{X}$, and therefore

$$\mathbf{1}\{f(x) \leq m_n\} \rightarrow \mathbf{1}\{f(x) = f(x^*)\} \quad \text{for all } x \in \mathbb{X}. \quad (72)$$

Moreover, $0 \leq \mathbf{1}\{f(x) \leq m_n\} \leq 1$, so dominated convergence with respect to μ gives

$$\mathbb{P}_n(f(X) \leq m_n) = \mathbb{E}_n[\mathbf{1}\{f(X) \leq m_n\}] \rightarrow \mathbb{E}_n[\mathbf{1}\{f(X) = f(x^*)\}] = \mu(\{x \in \mathbb{X} : f(x) = f(x^*)\}) \quad \text{a.s.} \quad (73)$$

Combining (71) with (73) and taking \limsup yields (69). The last statement follows when

$$\mu(\{x \in \mathbb{X} : f(x) = f(x^*)\}) = 0. \quad (74)$$

□

Interpretation. Proposition D.1 is a population statement with an auxiliary draw $X \sim \mu$ (independent of \mathcal{D}_n). It implies that, when the set of global minimizers has μ -measure 0, enforcing occurrence calibration at m_n forces $\hat{F}_n(m_n | X)$ to be small for μ -almost all X at large n .

The result does not describe how the predictive lower tail behaves in the region explored by the BO policy. This motivates calibrating below a higher threshold t_n and using notions based on the truncated CDF $\hat{F}_{n,t_n}(\cdot | x)$.

E. Implementation Details

E.1. GP Matérn Model and Parameters

In the experiment reported Section 6, the GP model $\text{GP}(m, k)$ is such that the mean function is constant over \mathbb{X} , $m(x) = \mu$ for $x \in \mathbb{X}$. The kernel k is selected from the anisotropic Matérn kernel family. The anisotropic Matérn kernel family is defined, for $x, y \in \mathbb{R}^d$, as

$$k_{\sigma, \nu, \rho}(x, y) = \sigma^2 \kappa_\nu(h), \quad h^2 = \sum_{i=1}^d \frac{(x_{[i]} - y_{[i]})^2}{\rho_i^2}, \quad (75)$$

where σ^2 is the variance parameter, $\rho = (\rho_1, \dots, \rho_d)$ are component-wise lengthscales, and κ_ν denotes the Matérn correlation function (Stein, 1999, Chapter 2.7). The smoothness parameter is fixed to $\nu = p + 1/2$ with $p \in \mathbb{N}^*$.

The parameter (μ, ρ, σ) is selected by maximum likelihood. In the Experiments in Section 6, $p = 2$.

E.2. Maximization of EI

EI is maximized with the sequential Monte Carlo (SMC) procedure of Feliot et al. (2016), available in `gprmp`. A population of particles is iteratively reweighted with EI-proportional weights and propagated through mutation steps, yielding a discrete approximation of the EI maximizers. The best particle is then used to initialize a local maximization with the *sequential least squares quadratic programming* (SLSQP) algorithm. This hybrid global–local procedure is applied for all methods. In the Experiments in Section 6 we used 1000 particles.

E.3. Bayesian Optimization with TCGP

Algorithm 1 summarizes EI-based BO with TCGP. It follows the procedure described in the main text. At iteration n , the empirical quantile $q_{\delta, n}$ is used as a candidate threshold when there is sufficient data support in the lower tail, and the previous threshold is kept otherwise. Concretely, we estimate the excursion probability below $q_{\delta, n}$ and enforce $\hat{p}_{q_{\delta, n}, n}^w \geq p_{\min}$. If the condition fails, the threshold is frozen to avoid calibrating on too few points. Since the BO design is adaptive, this support rule is only a safeguard.

Density-ratio estimation and weights. The weighted LOO quantities in Section 4.2 aim at approximating μ -averages using the adaptively sampled BO locations $(X_i)_{i=1}^n$, which are not distributed according to μ . We use an empirical density-ratio correction as a heuristic for this adaptive design. If ν_n denotes the smoothed empirical design density of the BO locations, the idealized weights have the form

$$w_i \propto \frac{d\mu}{d\nu_n}(X_i), \quad (76)$$

and are used to approximate, for the integrands φ appearing in the weighted LOO criteria,

$$\int_{\mathbb{X}} \varphi(x) \mu(dx) \approx \sum_{i=1}^n \tilde{w}_i \varphi(X_i), \quad \tilde{w}_i = \frac{w_i}{\sum_{j=1}^n w_j}. \quad (77)$$

In our experiments, μ is uniform on \mathbb{X} , hence

$$w_i \propto \frac{1}{\nu_n(X_i)}. \quad (78)$$

In practice, we use a KDE estimate $\hat{\nu}_n$ of this design density. Concretely, we rescale the design points X_i to $[0, 1]^d$ using the bounds of \mathbb{X} , and fit a Gaussian kernel density estimator (KDE) to the rescaled points (Scott, 1992). The bandwidth is chosen according to Scott’s rule (Scott, 1992). We then set

$$w_i \propto \frac{d\mu}{d\hat{\nu}_n}(X_i), \quad (79)$$

which reduces to $w_i \propto 1/\hat{\nu}_n(X_i)$ for uniform μ , and normalize to obtain $(\tilde{w}_i)_{i=1}^n$.

Large density ratios can lead to highly variable weights. A standard safeguard is weight clipping, for instance $w_i \leftarrow \min(w_i, w_{\max})$ for a fixed $w_{\max} > 0$, followed by renormalization. We did not use clipping in the reported experiments.

Algorithm 1 BO with TCGP

Require: Initial dataset $\mathcal{D}_{n_0} = \{(X_i, Z_i)\}_{i=1}^{n_0}$ with $Z_i = f(X_i)$, design space \mathbb{X} , budget N_{\max} , quantile level $\delta \in (0, 1]$, minimum excursion probability $p_{\min} > 0$.

Ensure: Best value $m_{N_{\max}}$ and associated point X_{\min} .

- 1: Set $n \leftarrow n_0$.
- 2: Set $m_n \leftarrow \min_{1 \leq i \leq n} Z_i$ and choose any $X_{\min} \in \arg \min_{1 \leq i \leq n} Z_i$.
- 3: Set the current threshold $t \leftarrow q_{\delta, n}$.
- 4: **while** $n < N_{\max}$ **do**
- 5: Fit a GP model to \mathcal{D}_n by maximum likelihood and obtain functions $x \mapsto f_n(x)$ and $x \mapsto \sigma_n(x)$.
- 6: Estimate the importance weights $(\tilde{w}_i)_{i=1}^n$ (Section 4.2 and paragraph below).
- 7: Set $\tilde{t} \leftarrow q_{\delta, n}$.
- 8: Compute the weighted excursion frequency

$$\hat{p}_{\tilde{t}, n}^w = \sum_{i=1}^n \tilde{w}_i \mathbf{1}\{Z_i \leq \tilde{t}\}.$$

- 9: **if** $\hat{p}_{\tilde{t}, n}^w \geq p_{\min}$ **then**
- 10: Update $t \leftarrow \tilde{t}$.
- 11: **end if**
- 12: Select (β_n, λ_n) by minimizing $J_{t, n}^{\text{LOO}, w}$ on $[\beta_0, \beta_1] \times [\lambda_0, \lambda_1]$ (Section 5.1 and paragraph below).
- 13: Define EI ρ_n using the TCGP predictive CDFs with parameters (β_n, λ_n) (Section 5.2).
- 14: Choose $X_{n+1} \in \arg \max_{x \in \mathbb{X}} \rho_n(x)$ (paragraph below).
- 15: Evaluate $Z_{n+1} = f(X_{n+1})$ and set $\mathcal{D}_{n+1} \leftarrow \mathcal{D}_n \cup \{(X_{n+1}, Z_{n+1})\}$.
- 16: **if** $Z_{n+1} < m_n$ **then**
- 17: Set $m_{n+1} \leftarrow Z_{n+1}$ and $X_{\min} \leftarrow X_{n+1}$.
- 18: **else**
- 19: Set $m_{n+1} \leftarrow m_n$.
- 20: **end if**
- 21: Set $n \leftarrow n + 1$.
- 22: **end while**
- 23: **Return** $(X_{\min}, m_{N_{\max}})$.

Selection of (β_n, λ_n) . We minimize $J_{t, n}^{\text{LOO}, w}$ with a two-stage procedure. First, we sample (β, λ) uniformly on $[\beta_0, \beta_1] \times [\lambda_0, \lambda_1]$ (900 candidates) and select the best pair $(\tilde{\beta}, \tilde{\lambda})$ according to $J_{t, n}^{\text{LOO}, w}$. Second, we refine with the Nelder–Mead algorithm (Nelder & Mead, 1965) initialized at $(\tilde{\beta}, \tilde{\lambda})$. The supremum over $u \in [0, 1]$ in $J_{t, n}^{\text{LOO}, w}$ is evaluated on a fixed grid of u values.

E.4. Test-Set Evaluation of μ -Calibration Metrics

When an independent evaluation set is available, μ -calibration metrics can be computed for $X \sim \mu$ without leave-one-out or reweighting. Let $(X'_j, Z'_j)_{j=1}^L$ with $X'_j \sim \mu$ i.i.d. and $Z'_j = f(X'_j)$, and assume that the predictive CDFs $\hat{F}_n(\cdot | x)$ are constructed from \mathcal{D}_n only.

Direct test-set estimators. Fix $t \in \mathbb{R}$. Define

$$U'_{t, j} = \begin{cases} \hat{F}_n(Z'_j | X'_j) / \hat{F}_n(t | X'_j), & Z'_j \leq t, \\ 1, & Z'_j > t, \end{cases} \quad (80)$$

with the convention that $\hat{F}_n(t | X'_j) > 0$ when $Z'_j \leq t$. Assume that $\sum_{j=1}^L \mathbf{1}\{Z'_j \leq t\} > 0$ and set

$$G'_{t, L}(u) = \frac{\sum_{j=1}^L \mathbf{1}\{Z'_j \leq t\} \mathbf{1}\{U'_{t, j} \leq u\}}{\sum_{j=1}^L \mathbf{1}\{Z'_j \leq t\}}, \quad J'_{\text{tKS-PIT}, L}(\hat{F}_n | t) = \sup_{u \in [0, 1]} |G'_{t, L}(u) - u|. \quad (81)$$

The excursion probability $p_t = \mathbb{P}(f(X) \leq t)$ is estimated by

$$\hat{p}_{t,L} = \frac{1}{L} \sum_{j=1}^L \mathbf{1}\{Z'_j \leq t\}, \quad (82)$$

and the corresponding occurrence discrepancy estimator is

$$r'_{t,L} = \left| \hat{p}_{t,L} - \frac{1}{L} \sum_{j=1}^L \hat{F}_n(t | X'_j) \right|. \quad (83)$$

SMC-based estimators for small thresholds. For small t (in particular $t = m_n$ at later BO iterations), direct sampling from μ yields too few points with $f(X) \leq t$ to estimate $G_{\mu,t}$ and p_t accurately. We therefore use subset simulation implemented via sequential Monte Carlo (SMC) (Bect et al., 2017) to obtain particles approximately distributed according to $\mu(\cdot | f(X) \leq t)$ and an estimate of $p_t = \mathbb{P}(f(X) \leq t)$.

At the initial iteration with n_0 observations, we run subset simulation down to $t = m_{n_0}$ to compute an estimate $\hat{p}_{m_{n_0}}$ and a particle cloud $(\tilde{X}_i^{(0)})_{i=1}^m \approx \mu(\cdot | f(X) \leq m_{n_0})$. We evaluate tKS–PIT at m_{n_0} using $(\tilde{X}_i^{(0)})_{i=1}^m$, and we evaluate the occurrence discrepancy using $\hat{p}_{m_{n_0}}$.

When BO produces a new best value $m_n < m_{n-1}$, we do not rerun subset simulation from scratch. We reuse the particles available at level m_{n-1} as an initial population and perform additional SMC steps targeting the new excursion set $\{x : f(x) \leq m_n\}$. This yields updated particles $(\tilde{X}_i^{(n)})_{i=1}^m \approx \mu(\cdot | f(X) \leq m_n)$ together with an updated estimate \hat{p}_{m_n} . The particle cloud is used to form the empirical distribution of the μ -tPIT below m_n (and hence tKS–PIT), while \hat{p}_{m_n} is used in the occurrence discrepancy.

In all experiments, we use $m = 1000$ particles and Metropolis–Hastings moves for the Markov transition steps.

E.5. Reweighting for BCRGP

The BCRGP approach of Pion & Vazquez (2025) specifies a generalized normal model for standardized residuals and places a uniform prior on $\theta = (\beta, \lambda)$. We recall the resulting posterior construction and describe how we incorporate importance weights to target μ -probabilistic calibration over \mathbb{X} . In our experiments, global calibration diagnostics for BCRGP are reported using KS–PIT, i.e., the limit of tKS–PIT as $t \rightarrow \infty$.

Let $R_{n,-i}(X_i)$ denote the leave-one-out standardized residual at X_i ,

$$R_{n,-i}(X_i) = \frac{Z_i - f_{n,-i}(X_i)}{\sigma_{n,-i}(X_i)}, \quad (84)$$

where $f_{n,-i}$ and $\sigma_{n,-i}$ are the GP predictive mean and standard deviation obtained from $\mathcal{D}_n \setminus \{(X_i, Z_i)\}$. Let $p(r | \theta)$ be the density of $\mathcal{GN}(\beta, 0, \lambda)$ evaluated at r .

With a uniform prior on $(0, a) \times (0, b)$, BCRGP defines

$$p(\theta | \{R_{n,-i}(X_i)\}_{i=1}^n) \propto \prod_{i=1}^n p(R_{n,-i}(X_i) | \theta) \mathbf{1}\{0 < \beta < a\} \mathbf{1}\{0 < \lambda < b\}. \quad (85)$$

Let $\hat{\nu}_n$ be the density estimate used above. To incorporate importance weights, we replace the standard likelihood by a weighted likelihood, following Shimodaira (2000). Let $(\omega_i)_{i=1}^n$ be nonnegative weights proportional to $d\mu/d\hat{\nu}_n(X_i)$ (Section 4.2). For the weighted likelihood, the global scale of the exponents affects posterior concentration, so we fix the normalization

$$\bar{w}_i = n \omega_i / \sum_{j=1}^n \omega_j, \quad \sum_{i=1}^n \bar{w}_i = n. \quad (86)$$

The resulting pseudo-posterior is

$$p_w(\theta | \{R_{n,-i}(X_i)\}_{i=1}^n) \propto \prod_{i=1}^n p(R_{n,-i}(X_i) | \theta)^{\bar{w}_i} \mathbf{1}\{0 < \beta < a\} \mathbf{1}\{0 < \lambda < b\}. \quad (87)$$

Given Monte Carlo samples $(\beta_i, \lambda_i)_{i=1}^m$, Pion & Vazquez (2025) derive a Bayesian selection rule for (β^*, λ^*) targeting probabilistic calibration, quantified by the KS–PIT up to a prescribed quantile. To limit computational cost, we set $m = 200$ in this work; increasing m further had negligible impact on BO performance.

E.6. Experimental Parameter Settings

We summarize below the main parameters used in all numerical experiments.

Test-set evaluation parameters

- Test-set evaluation of calibration metrics: The subset simulation procedure uses $k_0 = 1000$ particles to estimate $P(f(X) \leq m_n)$ and to generate samples from $\mu(\cdot \mid f(X) \leq m_n)$.
- Occurrence discrepancy: The occurrence discrepancy r_t is computed using an additional $k_1 = 1000$ points sampled uniformly over \mathbb{X} .
- tKS–PIT computation: To compute the tKS–PIT, we subsample $k_2 = 900$ particles from the subset simulation output, ensuring that all corresponding function values lie below the current threshold m_n at each iteration.

Model parameters

- GP prior regularity: We use a Matérn covariance kernel with smoothness parameter $\nu = p + \frac{1}{2}$, with $p = 2$, corresponding to twice mean-square differentiable sample paths. All GP hyperparameters are estimated by maximum likelihood.
- Parameter bounds for calibration: The calibration parameters are constrained to

$$\lambda \in [\lambda_0, \lambda_1] = [5 \times 10^{-3}, 10], \quad \beta \in [\beta_0, \beta_1] = [0.1, 10].$$

- $p_{\min} = 0.015$.

E.7. Test Functions Used in the Experiments

Name	Domain	Expression of $f(x)$
Goldstein–Price	$[-2, 2]^2$	$(1 + (x_1 + x_2 + 1)^2(19 - 14x_1 + 3x_1^2 - 14x_2 + 6x_1x_2 + 3x_2^2))(30 + (2x_1 - 3x_2)^2(18 - 32x_1 + 12x_1^2 + 48x_2 - 36x_1x_2 + 27x_2^2))$
Rosenbrock	$[-5, 10]^d$	$\sum_{i=1}^{d-1} [100(x_{i+1} - x_i^2)^2 + (x_i - 1)^2]$
Ackley	$[-32.768, 32.768]^d$	$-20 \exp\left(-0.2\sqrt{\frac{1}{d} \sum_i x_i^2}\right) - \exp\left(\frac{1}{d} \sum_i \cos(2\pi x_i)\right) + 20 + e$
Dixon–Price– d	$[-10, 10]^d$	$(x_1 - 1)^2 + \sum_{i=2}^d i(2x_i^2 - x_{i-1})^2$
Hartmann– d	$[0, 1]^d$	$-\sum_{i=1}^d c_i^{(d)} \exp(-\sum_{j=1}^d a_{ij}^{(d)} (x_j - p_{ij}^{(d)})^2)$
Michalewicz– d	$[0, \pi]^d$	$-\sum_{i=1}^d \sin(x_i) \sin^{2m}(ix_i^2/\pi)$
Cross-In-Tray	$[-10, 10]^2$	$-0.0001 \left(\left \sin(x_1) \sin(x_2) \exp\left(\left 100 - \frac{\sqrt{x_1^2 + x_2^2}}{\pi} \right \right) \right + 1 \right)^{0.1}$
Shekel– m	$[0, 10]^4$	$-\sum_{i=1}^m \left(\sum_{j=1}^4 (x_j - C_{ji})^2 + \beta_i \right)^{-1}$
Perm– d	$[-d, d]^d$	$\sum_{i=1}^d \left(\sum_{j=1}^d (j + \beta_P) \left(x_j^i - \frac{1}{j^i} \right) \right)^2$

Table 1. Test functions used in the numerical experiments. Each function is continuous, deterministic, and defined on the domain \mathbb{X} . Expressions and domains follow the standard definitions provided in Surjanovic & Bingham (2013), with parameter values specified below.

Hartmann parameters.

$$a^{(3)} = \begin{bmatrix} 3.0 & 10.0 & 30.0 \\ 0.1 & 10.0 & 35.0 \\ 3.0 & 10.0 & 30.0 \\ 0.1 & 10.0 & 35.0 \end{bmatrix}, \quad c^{(3)} = \begin{bmatrix} 1.0 \\ 1.2 \\ 3.0 \\ 3.2 \end{bmatrix}, \quad p^{(3)} = 10^{-4} \begin{bmatrix} 3689 & 1170 & 2673 \\ 4699 & 4387 & 7470 \\ 1091 & 8732 & 5547 \\ 381 & 5743 & 8828 \end{bmatrix}.$$

$$a^{(6)} = \begin{bmatrix} 10 & 3 & 17 & 3.5 & 1.7 & 8 \\ 0.05 & 10 & 17 & 0.1 & 8 & 14 \\ 3 & 3.5 & 1.7 & 10 & 17 & 8 \\ 17 & 8 & 0.05 & 10 & 0.1 & 14 \end{bmatrix}, \quad c^{(6)} = \begin{bmatrix} 1.0 \\ 1.2 \\ 3.0 \\ 3.2 \end{bmatrix}, \quad p^{(6)} = 10^{-4} \begin{bmatrix} 1312 & 1696 & 5569 & 124 & 8283 & 5886 \\ 2329 & 4135 & 8307 & 3736 & 1004 & 9991 \\ 2348 & 1451 & 3522 & 2883 & 3047 & 6650 \\ 4047 & 8828 & 8732 & 5743 & 1091 & 381 \end{bmatrix}.$$

Michalewicz parameter.

$$m = 10$$

Perm parameter.

$$\beta_P = 1$$

Shekel parameters.

$$\beta = \frac{1}{10} (1, 2, 2, 4, 4, 6, 3, 7, 5, 5)^T$$

$$C = \begin{bmatrix} 4 & 1 & 8 & 6 & 3 & 2 & 5 & 8 & 6 & 7 \\ 4 & 1 & 8 & 6 & 7 & 9 & 3 & 1 & 2 & 3.6 \\ 4 & 1 & 8 & 6 & 3 & 2 & 5 & 8 & 6 & 7 \\ 4 & 1 & 8 & 6 & 7 & 9 & 3 & 1 & 2 & 3.6 \end{bmatrix}.$$

F. Additional Experiments

F.1. Running Time of the Methods

In this section, we report the per-iteration time required to train the GP or calibrated model (excluding sampling criteria maximization). All calibration methods have a similar computation time relatively to GP, but REGP is more costly (by a factor 10).

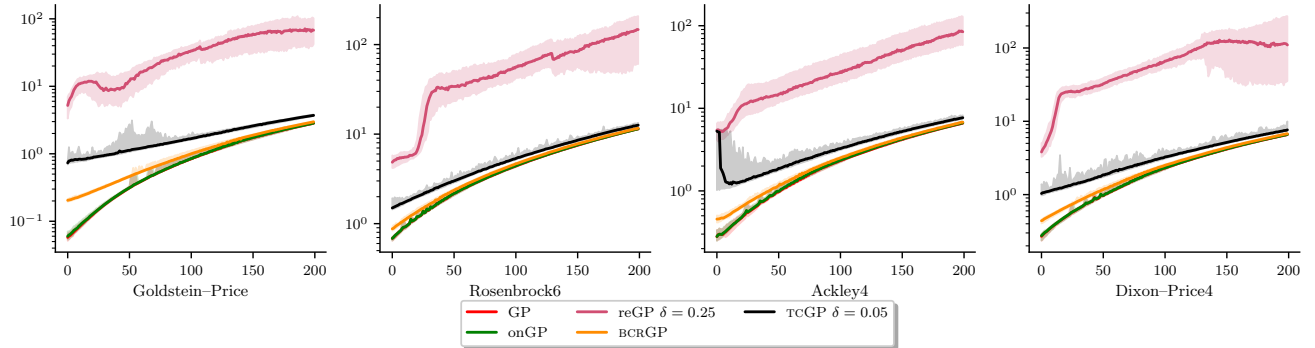


Figure 4. Training time for REGP, GP, TCGP, onGP, BCRGP at each iteration of BO.

F.2. Alternative Selection Criteria for TCGP

We compare several objectives for selecting (β, λ) in TCGP, with the aim of controlling thresholded μ -calibration and occurrence calibration below $t = q_{\delta, n}$. Rule 0 is the criterion J defined in (18). Figure 5 reports BO results over 100 iterations with $\delta = 0.1$.

A natural variant of (18) replaces the target $u \mapsto u \kappa_t^{\beta, \lambda}$ by the truncated map

$$u \mapsto \min \left(u \kappa_t^{\beta, \lambda}, 1 \right). \quad (88)$$

When $\kappa_t^{\beta, \lambda} > 1$, truncation saturates the target at 1. Large values of $\kappa_t^{\beta, \lambda}$ then become weakly penalized, and the objective can become insensitive to overestimation of lower-tail mass. We do not use this variant.

Rule 1. Multiply the weighted LOO tKS-PIT metric by the occurrence discrepancy:

$$J^{(1)}(\beta, \lambda) = J_{\text{tKS-PIT}, n}^{\text{LOO}, w} \left(\hat{F}_n^{\beta, \lambda} \mid t \right) r_t. \quad (89)$$

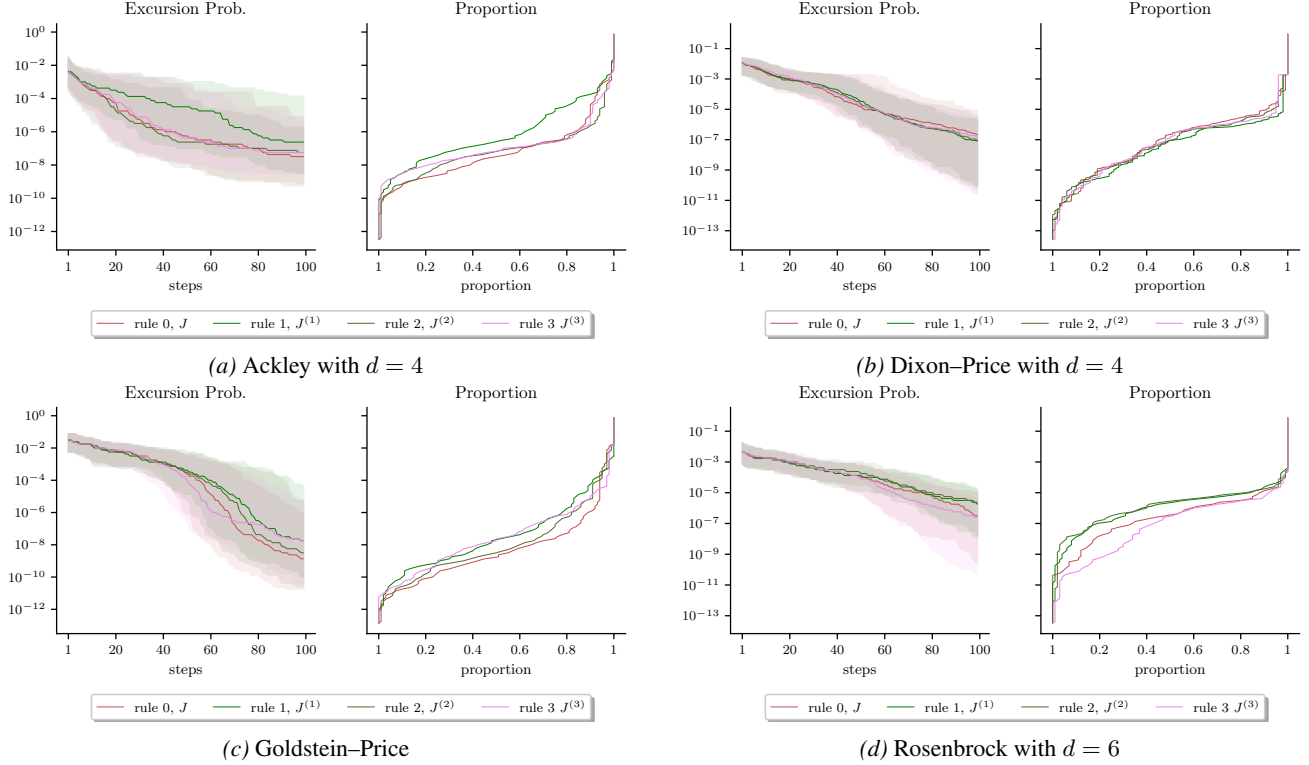


Figure 5. Comparison of TCGP variants. Left: median and 10%/90% quantiles of $p_{m_n} = \mathbb{P}(f(X) \leq m_n)$, where m_n is the best observed value after n evaluations and $X \sim \mu$. Right: fraction of runs reaching the prescribed target value.

Rule 2. Following Allen et al. (2025), define

$$c_t(u) = \frac{\mathbb{P}_n \left(U_t^{\beta, \lambda} \leq u \mid f(X) \leq t \right)}{\kappa_t^{\beta, \lambda}}. \quad (90)$$

Then use the KS-type deviation

$$J^{(2)}(\beta, \lambda) = \sup_{u \in [0, 1]} |c_t(u) - u|. \quad (91)$$

Rule 3. Compare the conditional tPIT curve to the rescaled map $u \mapsto u/\kappa_t^{\beta, \lambda}$:

$$J^{(3)}(\beta, \lambda) = \sup_{u \in [0, 1]} \left| \mathbb{P}_n \left(U_t^{\beta, \lambda} \leq u \mid f(X) \leq t \right) - \frac{u}{\kappa_t^{\beta, \lambda}} \right|. \quad (92)$$

Choice of objective. Figure 5 reports BO performance for the different selection rules. Performance is summarized by $p_{m_n} = \mathbb{P}(f(X) \leq m_n)$, where m_n is the best value observed after n evaluations and $X \sim \mu$ (with μ uniform), and by the fraction of runs reaching the prescribed target.

Empirically, the rules yield similar results overall. Rule 0 is used in the main experiments because it is the most consistent across the considered test functions. In particular, it behaves well on both highly multimodal landscapes (e.g., Ackley with $d = 4$) and on difficult smooth landscapes (e.g., Goldstein–Price). The alternative rules can either overweight tail-rank calibration, which can degrade optimization on smoother problems, or penalize overly optimistic lower-tail mass too weakly on multimodal problems. Rule 0 keeps a direct penalty on deviations of $\kappa_t^{\beta, \lambda}$ from 1 without additional tuning.

E.3. Effect of the Choice of δ for REGP on BO Performance

Figure 6 studies the sensitivity of REGP to the threshold parameter δ . BO performance is summarized by $p_{m_n} = \mathbb{P}(f(X) \leq m_n)$, where m_n is the best value observed after n evaluations and $X \sim \mu$ (with μ uniform), and by the fraction of runs

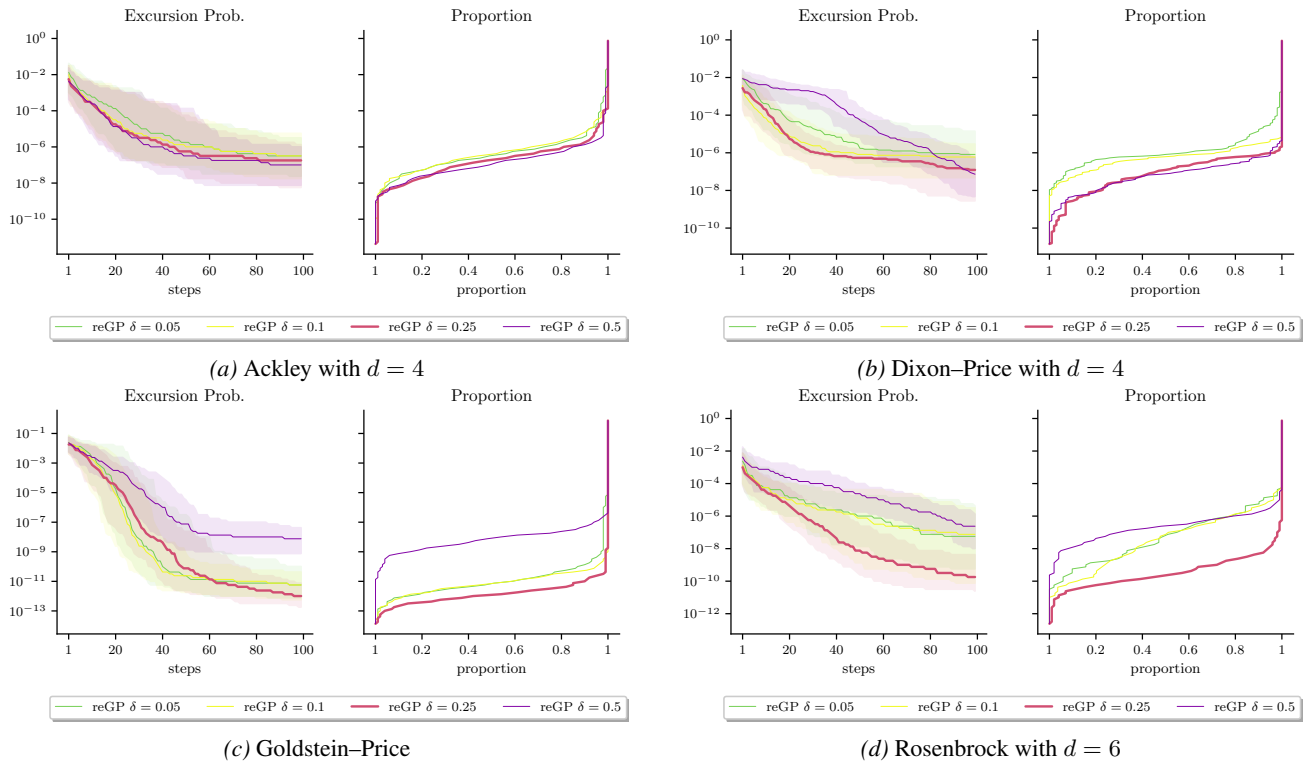


Figure 6. Sensitivity of REGP to δ (results shown after $n = 100$ BO iterations). Left: median and 10%/90% quantiles of $p_{m_n} = \mathbb{P}(f(X) \leq m_n)$, where m_n is the best value observed after n evaluations and $X \sim \mu$. Right: fraction of runs reaching the prescribed target level.

reaching the prescribed target.

Empirically, a large value of δ (e.g., $\delta = 0.5$) consistently leads to degraded performance across the considered problems. In contrast, $\delta = 0.25$ achieves the best overall performance and is consistently comparable to, or better than, smaller values such as $\delta = 0.05$ and $\delta = 0.1$. We therefore use $\delta = 0.25$ for all REGP experiments.

F.4. Effect of the Choice of δ for TCGP on BO Performance

Figure 7 studies the influence of the threshold parameter δ on TCGP. Performance is summarized by $p_{m_n} = \mathbb{P}(f(X) \leq m_n)$, where m_n is the best value observed after n evaluations and $X \sim \mu$ (with μ uniform), and by the fraction of runs reaching the prescribed target.

Empirically, $\delta = 0.05$ provides the most robust behavior across the considered problem classes. Larger values (e.g., $\delta = 0.25$) can yield the best performance on difficult but convex functions such as Goldstein–Price, although $\delta = 0.05$ remains competitive there. On highly multimodal, nonconvex problems such as Ackley, smaller values of δ perform substantially better. We therefore use $\delta = 0.05$ for all TCGP experiments.

F.5. Calibration on a Fixed Dataset

F.5.1. CALIBRATION BELOW THE PRESCRIBED THRESHOLD

We evaluate whether TCGP, either with the combined objective or with objectives targeting only thresholded or occurrence calibration, improves calibration at the operational threshold $t_n = q_{n,\delta}$ used to select (β, λ) , with $\delta \in \{0.25, 0.1, 0.05\}$.

The GP setup matches Section 6, except that we work with a fixed training dataset \mathcal{D}_n of size $n = 30d$ obtained from uniform sampling on \mathbb{X} . For each test function, we generate 100 independent datasets and report averages over the replicates.

For a given δ , calibration and predictive quality below $q_{n,\delta}$ are assessed using three metrics: twCRPS (jointly measuring

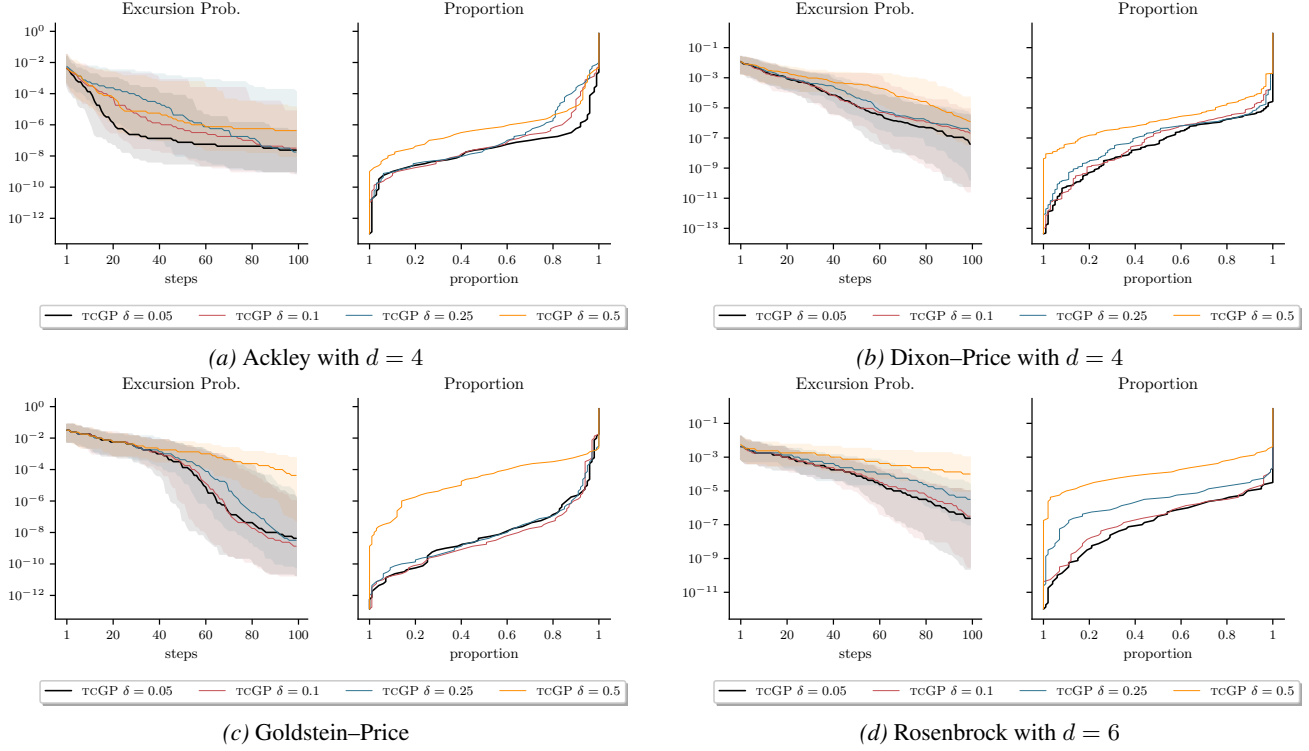


Figure 7. Sensitivity of TCGP to δ (results shown after $n = 100$ BO iterations). Left: median and 10%/90% quantiles of $p_{m_n} = \mathbb{P}(f(X) \leq m_n)$, where m_n is the best value observed after n evaluations and $X \sim \mu$. Right: fraction of runs reaching the prescribed target level.

calibration and sharpness below $q_{n,\delta}$, r_t (occurrence calibration at t_n), and tKS-PIT (thresholded μ -calibration below t_n). The tKS-PIT is computed using 4000 points sampled conditional on $f(x) \leq q_{n,\delta}$ by subset simulation (see Section 2 of Bect et al., 2017). In addition, 4000 points are sampled uniformly on \mathbb{X} to estimate r_t and twCRPS.

Results are reported in Table 2. Overall, TCGP improves both r_t and tKS-PIT for all values of δ , with smaller gains in twCRPS. The local variant TCGP-thres consistently improves tKS-PIT, but can worsen r_t on some problems (e.g., Hartman with $d = 6$ and Ackley with $d = 4$). The marginal variant TCGP-occ improves r_t but degrades tKS-PIT on several test functions. For Ackley, TCGP shows no improvement over the GP baseline for $\delta \in \{0.25, 0.1\}$, and only a limited gain for $\delta = 0.05$.

F.5.2. COMPARISON BETWEEN MULTIPLE METHODS

We evaluate whether REGP and TCGP improve calibration below the current best value m_n relative to a standard GP model. As above, we consider a fixed training dataset \mathcal{D}_n of size $n = 30d$ obtained from uniform sampling on \mathbb{X} . Results are reported in Table 3. Overall, both methods achieve improved or comparable calibration across the test functions, with REGP showing the largest gains on smooth (nearly convex) objectives and TCGP on the more challenging functions.

On Ackley, we observe a marked improvement in both tKS-PIT and r_t evaluated at m_n relative to the other methods, while improvements at the calibration threshold $t = q_{n,\delta}$ (with $\delta = 0.05$) were more limited. This suggests that calibration below an operational threshold t_n can still translate into substantial gains at more extreme levels $t \leq t_n$. A similar pattern is observed on Hartman6.

F.6. Additional Results for EI and UCB

F.6.1. ADDITIONAL RESULTS FOR EI

In this section, we report results on additional test functions in Figures 8 and 9. BO performance is summarized using two complementary views: the attained-level probability $p_{m_n} = \mathbb{P}(f(X) \leq m_n)$, where m_n is the best observed value after n

Method	Goldstein Price			Rosenbrock6			Hartman6			Dixon Price 4			Ackley4		
	twCRPS	r_t	tKS-PIT	twCRPS	r_t	tKS-PIT	twCRPS	r_t	tKS-PIT	twCRPS	r_t	tKS-PIT	twCRPS	r_t	tKS-PIT
$n = 30, t = q_{n,\delta}, \delta = 0.25$															
GP	6.9e2	0.04	0.64	6.0e3	0.01	0.16	0.049	0.095	0.15	2.7e2	0.0059	0.16	0.12	0.093	0.14
TCGP	5.7e2	0.036	0.27	6.0e3	0.01	0.14	0.052	0.06	0.28	2.6e2	0.0059	0.13	0.12	0.027	0.24
TCGP-occ	6.1e2	0.036	0.52	8.9e3	0.0095	0.36	0.059	0.046	0.79	4.3e2	0.0071	0.42	0.13	0.018	0.51
TCGP-thres	5.8e2	0.036	0.27	6e3	0.01	0.14	0.05	0.11	0.15	2.6e2	0.0059	0.13	0.12	0.078	0.13
$n = 30, t = q_{n,\delta}, \delta = 0.1$															
GP	6.0e2	0.11	0.83	2.8e3	0.011	0.3	0.027	0.018	0.27	1.1e2	0.0047	0.22	0.063	0.042	0.19
TCGP	5.1e2	0.065	0.48	2.8e3	0.011	0.27	0.027	0.021	0.24	1.0e2	0.0051	0.19	0.066	0.021	0.25
TCGP-occ	5.2e2	0.065	0.68	3.4e3	0.011	0.58	0.031	0.01	0.67	1.6e2	0.0057	0.44	0.071	0.012	0.52
TCGP-thres	5.1e2	0.065	0.41	2.9e3	0.011	0.27	0.031	0.096	0.12	1.0e2	0.0053	0.19	0.085	0.12	0.19
$n = 30, t = q_{n,\delta}, \delta = 0.05$															
GP	5.8e2	0.16	0.91	1.8e3	0.023	0.39	0.016	0.0088	0.39	56	0.005	0.32	0.042	0.014	0.29
TCGP $\delta = 0.05$	5e2	0.089	0.65	1.8e3	0.02	0.34	0.016	0.016	0.18	55	0.0054	0.26	0.044	0.025	0.28
TCGP-occ	4.9e2	0.09	0.75	2.1e3	0.02	0.61	0.017	0.011	0.39	64	0.0056	0.48	0.045	0.011	0.42
TCGP-thres	4.9e2	0.089	0.62	1.8e3	0.02	0.31	0.023	0.09	0.15	56	0.0059	0.27	0.14	0.16	0.22

Table 2. Comparison of calibration using the twCRPS, r_t , and tKS-PIT below $t = q_{n,\delta}$ for $\delta \in \{0.25, 0.1, 0.05\}$ for TCGP with the combined objective, or with tKS-PIT (TCGP-thres), or r_t (TCGP-occ) to select the parameters, and standard GP, all calibrated below $q_{n,\delta}$. The twCRPS and r_t are evaluated on a test grid $(X_i, f(X_i))_{i=1}^m$, with $m = 4000$, and the X_i s are uniformly distributed. tKS-PIT is approximated using another test grid $(\tilde{X}_i, f(\tilde{X}_i))_{i=1}^m$, with $m = 4000$, where $f(\tilde{X}_i) \leq q_{n,\delta}$ and the \tilde{X}_i are sampled using a subset simulation algorithm (Bect et al., 2017).

Method	Goldstein Price			Rosenbrock6			Hartman6			Dixon Price 4			Ackley4		
	twCRPS	r_t	tKS-PIT	twCRPS	r_t	tKS-PIT	twCRPS	r_t	tKS-PIT	twCRPS	r_t	tKS-PIT	twCRPS	r_t	tKS-PIT
$n = 30$															
GP	5.7e2	0.2	0.99	6.8e2	0.036	0.77	0.0016	0.0043	0.61	16	0.015	0.83	0.012	0.0061	0.72
TCGP $\delta = 0.05$	4.9e2	0.12	0.78	6.2e2	0.027	0.56	0.0015	0.0033	0.33	14	0.011	0.68	0.012	0.0047	0.49
TCGP $\delta = 0.1$	4.8e2	0.12	0.72	6.3e2	0.03	0.62	0.0015	0.004	0.59	15	0.012	0.74	0.012	0.0059	0.66
TCGP $\delta = 0.25$	4.5e2	0.13	0.87	6.2e2	0.031	0.67	0.0016	0.0044	0.83	14	0.012	0.73	0.012	0.0063	0.64
REGP $\delta = 0.05$	1.9	0.021	0.77	39	0.0039	0.66	0.0042	0.0048	0.89	5.3	0.0047	0.74	0.013	0.0046	0.95
REGP $\delta = 0.1$	2.9	0.019	0.61	54	0.0035	0.43	0.0038	0.0038	0.84	11	0.0055	0.66	0.013	0.0043	0.89
REGP $\delta = 0.25$	6.7	0.029	0.69	4.1e2	0.018	0.79	0.0018	0.0032	0.72	25	0.015	0.82	0.012	0.006	0.76

Table 3. Comparison of calibration using the twCRPS, r_t , and tKS-PIT below $t = m_n$ for TCGP with multiple δ , REGP, and the standard GP. The calibration methods use thresholds based on $q_{n,\delta}$, while the metrics are evaluated at m_n . The twCRPS and r_t are evaluated on a test grid $(X_i, f(X_i))_{i=1}^m$, with $m = 4000$, and the X_i s are uniformly distributed. tKS-PIT is approximated using another test grid $(\tilde{X}_i, f(\tilde{X}_i))_{i=1}^m$, with $m = 4000$, where $f(\tilde{X}_i) \leq m_n$ and the \tilde{X}_i are sampled using a subset simulation algorithm (Bect et al., 2017).

iterations and $X \sim \mu$ (here μ is uniform on \mathbb{X}), and the fraction of runs that reach a prescribed target level.

Overall, REGP and TCGP consistently improve upon the standard GP baseline and typically outperform BCRGP and onGP. An exception is Ackley ($d = 10$), where onGP achieves the best performance. On the smoother (nearly convex) objectives, REGP and TCGP are the top-performing methods; on the Perm function, TCGP yields only modest gains over the GP baseline compared to REGP. On highly non-convex functions, TCGP most often provides the largest improvements.

Figure 10 reports diagnostic experiments on moderate-dimensional test functions ($d = 10$ to $d = 20$) over 150 BO iterations. These results extend the controlled benchmark evidence beyond the main text, but do not constitute a high-dimensional BO evaluation.

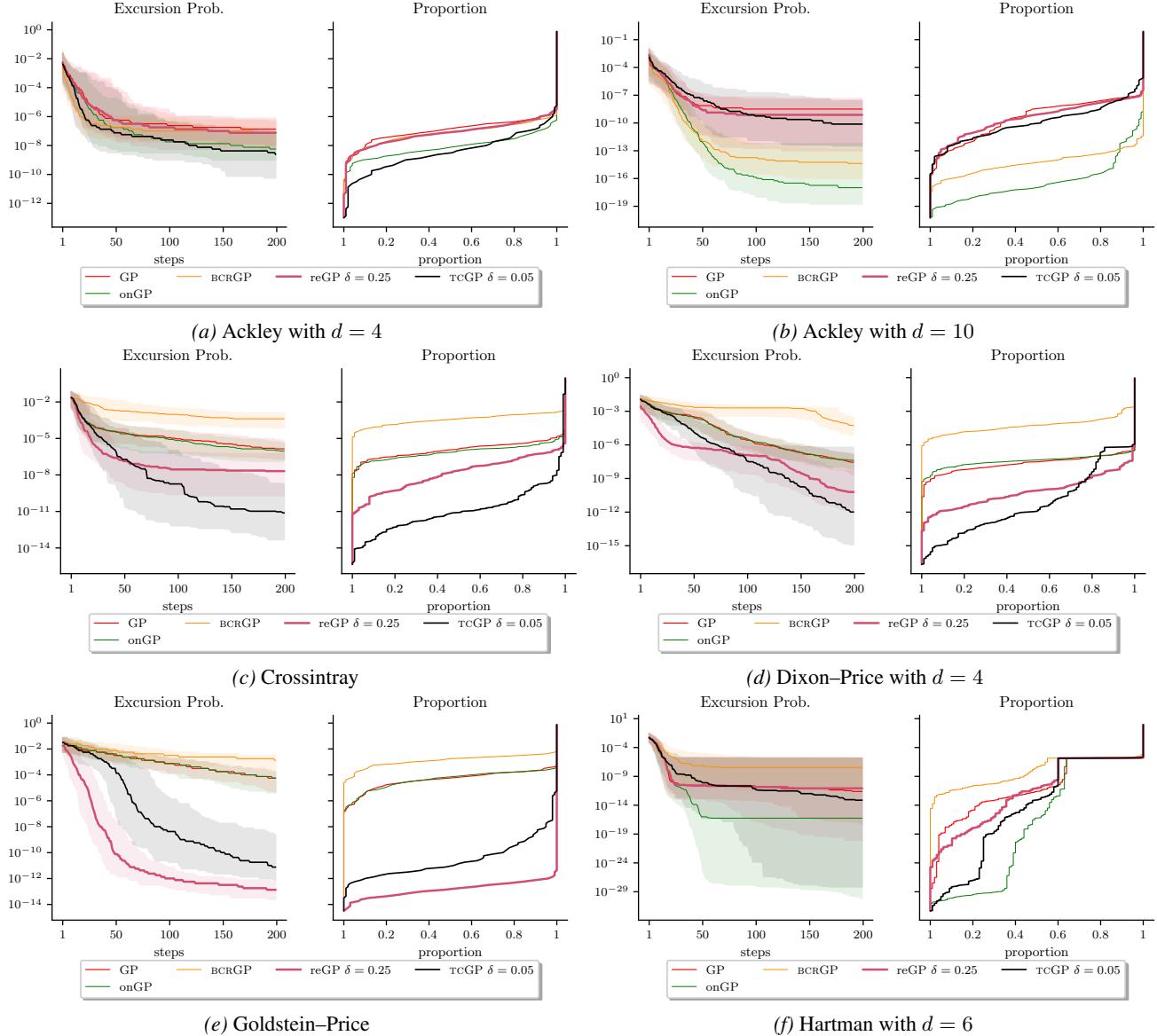


Figure 8. Comparison of the BO performance with EI as sampling criteria for GP, REGP with $\delta = 0.25$, onGP and TCGP with $\delta = 0.05$. Left: median and 10%/90% quantile of $p_{m_n} = P(f(X) \leq m_n)$, where m_n is the best observed value so far. Right: fraction of successful runs reaching a prescribed target level.

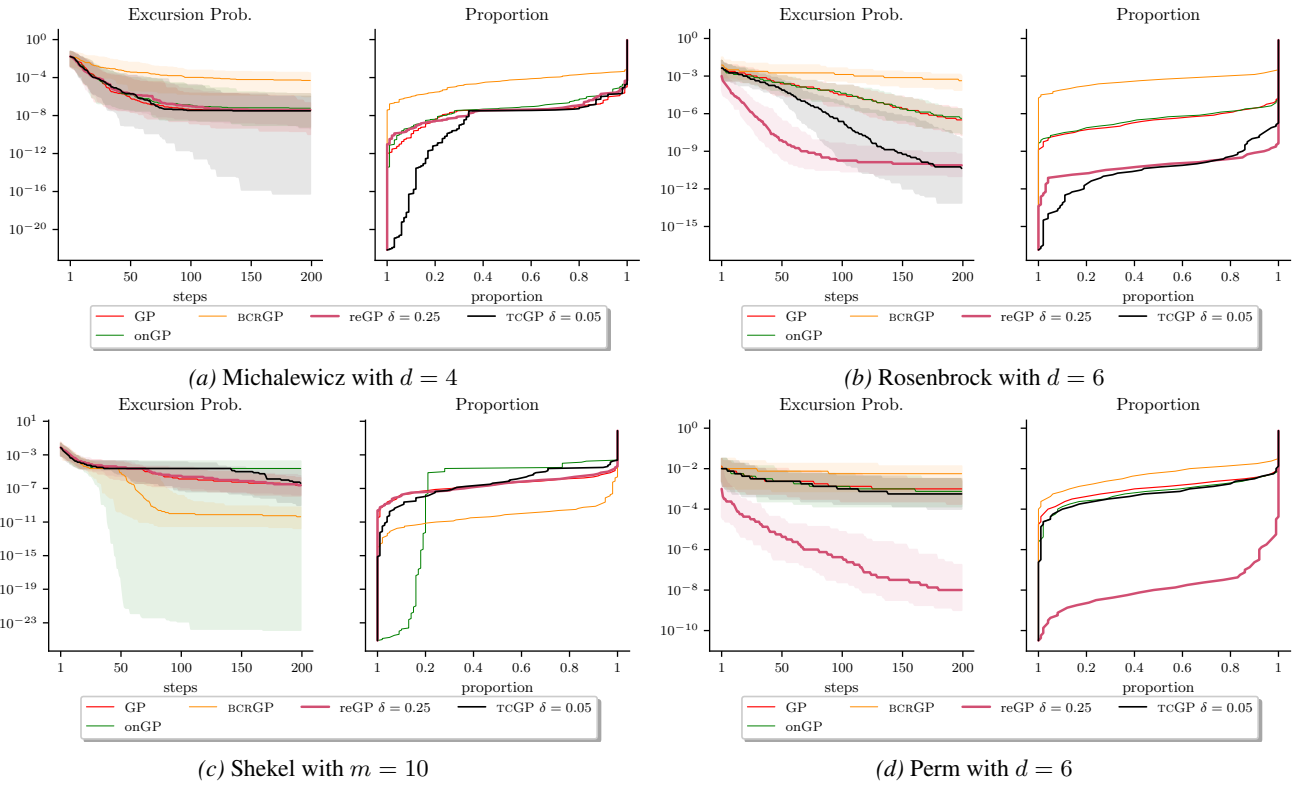


Figure 9. Comparison of the BO performance with EI as sampling criteria for GP, reGP with $\delta = 0.25$, onGP and tcGP with $\delta = 0.05$. Left: median and 10%/90% quantile of $p_{m_n} = \mathbb{P}(f(X) \leq m_n)$, where m_n is the best observed value so far. Right: fraction of successful runs reaching a prescribed target level.

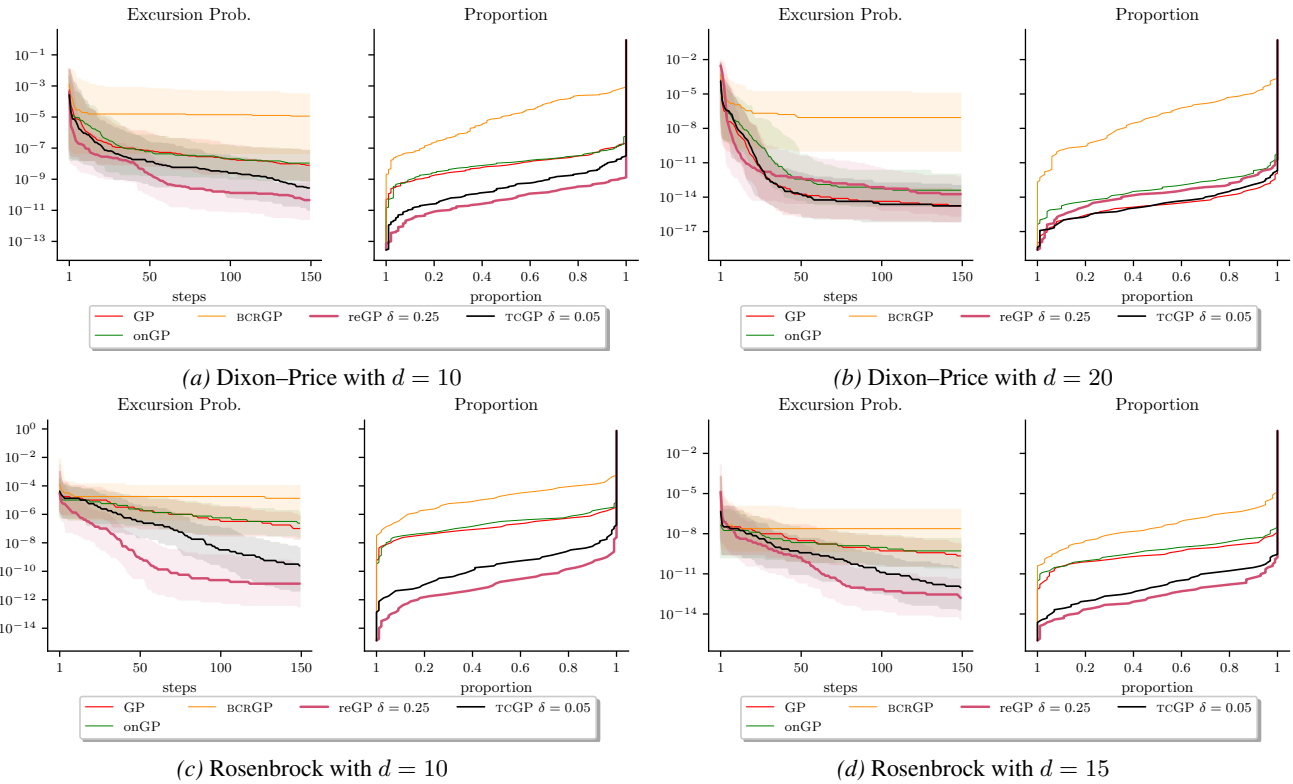


Figure 10. Comparison of the BO performance in moderate dimension $d = 10$ to $d = 20$ for 150 iterations with EI as sampling criteria for GP, REGP with $\delta = 0.25$, onGP and TCGP with $\delta = 0.05$. Left: median and 10%/90% quantile of $p_{m_n} = P(f(X) \leq m_n)$, where m_n is the best observed value so far. Right: fraction of successful runs reaching a prescribed target level.

F.6.2. RESULTS FOR UCB

We compare a standard GP model and TCGP using the upper confidence bound (UCB) sampling criterion (Lai & Robbins, 1985; Auer et al., 2002; Srinivas et al., 2010), to assess whether tail calibration also affects a criterion other than EI.

As above, BO performance is summarized by the probability of excursion $p_{m_n} = \mathbb{P}(f(X) \leq m_n)$, where m_n is the best observed value after n iterations, and by the fraction of runs reaching a prescribed target level, which provides a complementary view of method reliability.

UCB with a GP model. Fix $\varepsilon \in (0, 1]$. With a Gaussian predictive distribution, the $(1 - \varepsilon)$ lower confidence bound used for minimization is

$$f_n(x) - \Phi^{-1}(1 - \varepsilon) \sigma_n(x), \tag{93}$$

where Φ denotes the standard normal CDF.

UCB with TCGP. With TCGP parameters (β, λ) , the predictive distribution is generalized normal, and the corresponding $(1 - \varepsilon)$ lower confidence bound becomes

$$f_n(x) - \Theta_{\beta,0,1}^{-1}(1 - \varepsilon) \lambda \sigma_n(x), \tag{94}$$

where $\Theta_{\beta,0,1}$ is the CDF defined in (3).

Results are reported in Figures 11 and 12 with UCB and $\varepsilon = 0.1$. Overall, TCGP outperforms the GP baseline on most test functions. On Ackley ($d = 4$) the gains are modest and results are similar for Ackley ($d = 10$); in these cases UCB with a standard GP is already strong, making improvements harder to obtain.

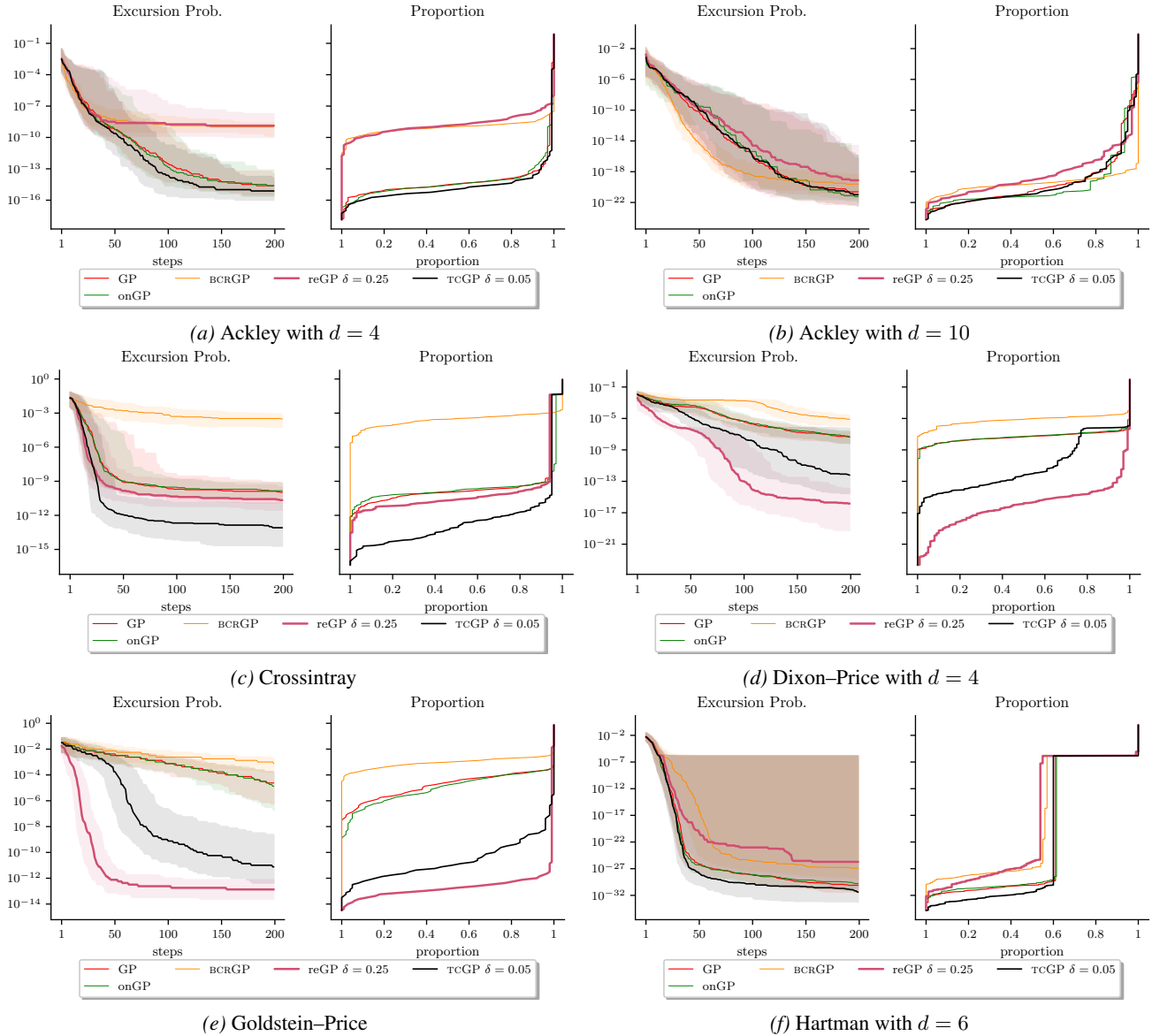


Figure 11. Comparison of the BO performance with UCB with $\varepsilon = 0.1$ as sampling criteria for GP, and TCGP with $\delta = 0.05$. Left: median and 10%/90% quantile of $p_{m_n} = \mathbb{P}(f(X) \leq m_n)$, where m_n is the best observed value so far. Right: fraction of successful runs reaching a prescribed target level.

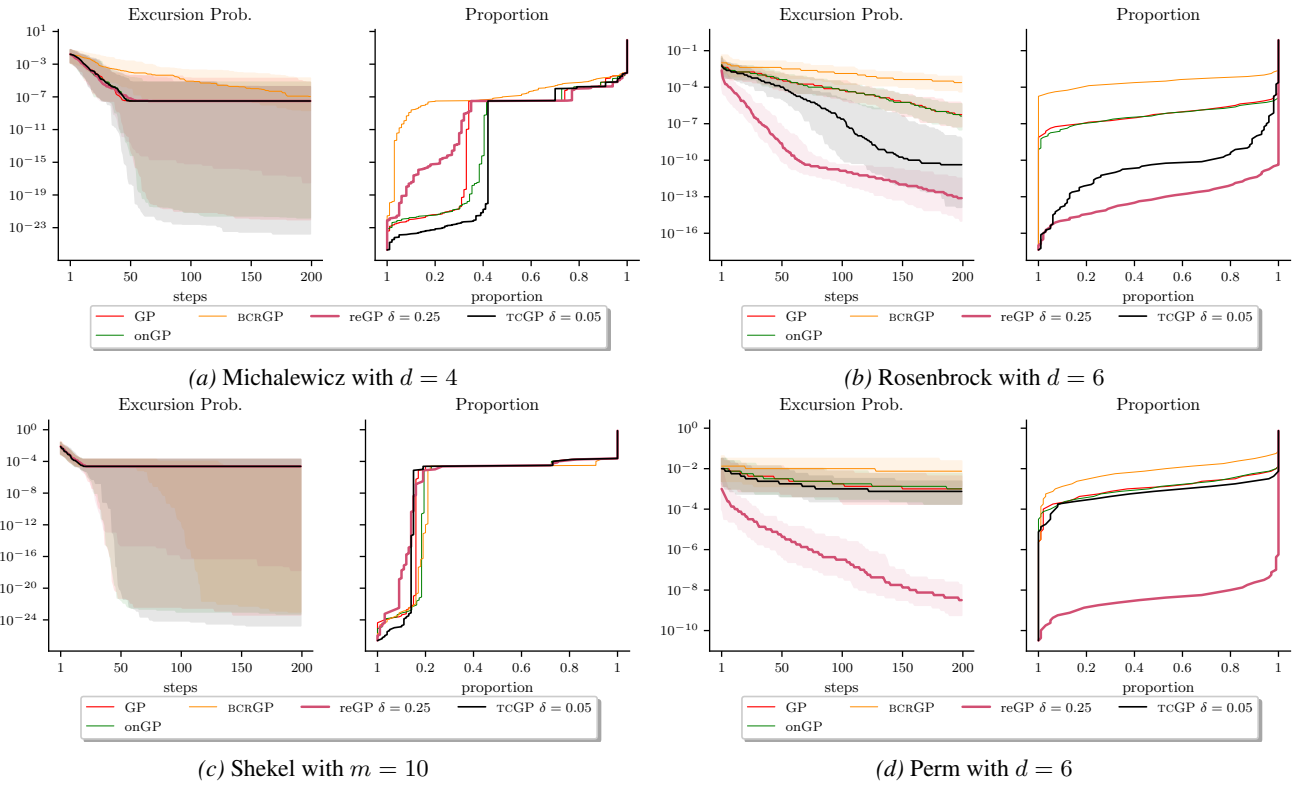


Figure 12. Comparison of the BO performance with UCB with $\varepsilon = 0.1$ as sampling criteria for GP, and TCGP with $\delta = 0.05$. Left: median and 10%/90% quantile of $p_{m_n} = \mathbb{P}(f(X) \leq m_n)$, where m_n is the best observed value so far. Right: fraction of successful runs reaching a prescribed target level.